Micrometrically Controlled Surface Modification of Teflon® by Redox Catalysis: Electrochemical Coupling between Teflon® and a Gold Band Ultramicroelectrode

Christian Amatore,*[a] Catherine Combellas,[b] Frédéric Kanoufi,[b] Catherine Sella,[a] André Thiébault,[b] and Laurent Thouin[a]

Abstract: Carbon–fluorine bonds of Teflon® (polytetrafluoroethylene, PTFE) can be reduced electrochemically with the purpose of modifying its adhesive and wetting surface properties by micrometrically controlled surface carbonization of the material. This can be performed adequately by redox catalysis provided that the redox mediator couple has a sufficiently negative reduction potential. The process is investigated kinetically with benzonitrile as the mediator and a gold-band ultramicroelectrode mounted adjacent to a PTFE block, though separated from it by an insulating micrometric mylar gap. For moderate fluxes of reduced mediator, the whole device behaves as a generator–collector double-band assembly with a constant current amplification factor. This is maintained over long periods of time, during which the carbonized PTFE zones extends over distances that are much wider than the slowly expanding cylindrical diffusion layer generated at the gold-microband electrode. This establishes that the overall redox catalysis proceeds through electronic conduction in the *n*-doped carbonized material. Thus, carbonization progresses at the external edge of the freshly carbonized surface in a diffusion-like fashion (dependence on the square root of time), while the redox-mediator oxidized form is regenerated at the carbonized PTFE edge facing to the gold ultramicroelectrode, so that the overall rate of carbonization is controlled by solution diffusion only. For larger fluxes of mediator, the heterogeneous rate of reduction and doping of PTFE becomes limiting, and the situation is more complex. A conceptually simple model is developed which predicts and explains all the main dynamic features of the system under these circumstances and allows the determination of the heterogeneous rate constant of carbon–fluorine bonds at the interface between the carbonized zone and the fresh PTFE. This model can be further refined to account for the effect of ohmic drop inside the carbonized zone on the heterogeneous reduction rate constants and henceforth gives an extremely satisfactory quantitative agreement with the experimental data.

Keywords: carbonization · catalysis · microelectrodes · polytetrafluoroethylene (PTFE) · reductions · redox chemistry · surface chemistry

Introduction

Polytetrafluoroethylene (PTFE or Teflon®) is a perfluorinated polymer with uncommonly small surface tension so that its wetting and adhesive abilities are extremely poor. These specific properties together with the great chemical stability of the carbon–carbon and carbon–fluorine bonds has led to numerous applications either at the industrial/professional or domestic scales. However, the same properties make it difficult to attach PTFE blocks together or to other materials, so that PTFE objects have generally to be cast into a single piece or carved from PTFE blocks, but cannot be glued/soldered/metallized as these processes are performed with other polymeric materials. It is therefore of importance to devise ways to modify the surface properties of PTFE blocks in a controlled fashion so that the material surface tension and chemical reactivity are changed locally.

In a detailed review, Kavan[1] describes how such surface modification can be performed by electrochemical reduction of the carbon–fluorine bonds. This may be performed by solvated electrons (see also refs. [2, 3]) or by generating radical anions in liquids or in solid electrolytes. PTFE surfaces may also be directly reduced in DMF/NBu_4BF_4 into a carbonized material by an electrode poised at a potential more negative than -2.5 V versus SCE and placed in straight contact with the PTFE.[4] These carbonization processes are

[a] Dr. C. Amatore, Dr. C. Sella, Dr. L. Thouin
Ecole Normale Supérieure, Département de Chimie
UMR CNRS 8640 "PASTEUR", 24 rue Lhomond
75231 Paris Cedex 05 (France)

[b] Dr. C. Combellas, Dr. F. Kanoufi, Dr. A. Thiébault
Ecole Supérieure de Physique et Chimie Industrielles
ERS 657
10 rue Vauquelin, 75231 Paris Cedex 05 (France)

0947-6539/00/0605-0820 $ 17.50+.50/0

reported to lead ultimately to a *n*-doped polymeric carbon material through a two stages reduction [Eqs. (1) and (2)].

$$-(CF_2)_n- + 2n\,e^- + 2n\,Cat^+ \longrightarrow -(C)_n- + 2n\,[Cat^+,F^-] \quad \text{(fast)} \qquad (1)$$

$$-(C)_n- + \delta n\,e^- + \delta n\,Cat^+ \longrightarrow [-(C^{\delta-})_n-,\delta n\,Cat^+] \quad \text{(slow)} \qquad (2)$$

In Equation (2), δ represents the excess of negative charge *per* carbon center in the carbonized matrix ($0.05 \leq \delta \leq 0.45$[4]). Therefore the reduced PTFE presents a significant electrical conductibility through electronic conduction and mobility of the cations. Because of this electrical conduction, when PTFE is adjacent to an electrode set at a sufficiently negative potential, reduction of the PTFE may occur far from the electrode/PTFE interface, at the outer edge of the carbonized zone either in surface of the PTFE block or within its bulk.[1, 4] Due to the necessity of cation diffusion–migration to compensate the generation of fluoride anions [Eq. (1)], extension of the carbonized zone occurs faster at the PTFE surface than within its bulk: propagation requires diffusion–migration of fluoride ions and cations through the carbonized bulk zone to and from the internal surface at which reduction of carbon fluorine bonds occur. As expected, the depth of reduction is reported to obey a diffusion-type law [namely, $h \propto (\kappa_h t)^{1/2}$, with κ_h (apparent diffusion coefficient) being smaller the larger the cation].[1, 4]

In this work, we wish to report a kinetic investigation of the above processes performed in the context of the reduction of PTFE by radical anions[5, 6] electrochemically generated in DMF in the presence of tetraalkylammonium supporting electrolyte [NR_4BF_4, R = Et, *n*Bu, *n*Hex (hexyl)]. The originality of the present study consists in the fact that the radical anions are generated in solution, at micrometric distance of the PTFE by a gold-band ultramicroelectrode mounted parallel to the PTFE block and separated from it by an insulating gap, in a way reminiscent of double-band ultramicroelectrode assemblies.[7–11]

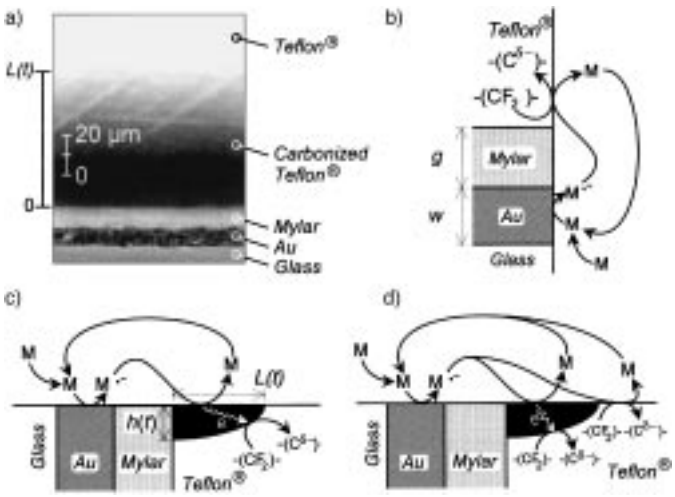

Figure 1. Schematic views of the microband assemblies used in this work and of their dynamics. For determination of I_{band} a second assembly is used in which the mylar sheet and PTFE block is replaced by a glass sheet. a) Optical microscopic view of the surface of the assembly showing from bottom to top, the glass plate substrate, the gold microband, the insulating mylar gap, the carbonized PTFE zone and the unaltered PTFE. b) Schematic cross-section of the assembly represented in a), showing the definition of *w* and g and describing the diffusional dynamics at short times. c) Schematic representation of the dynamics for low fluxes of mediator radical anion ($M^{\bullet -}$) and definition of *h* and *L*. The blackened elliptic area represents the carbonized zone (see text). Note that for the sake of simplicity the electron stoichiometry of reactions is not respected and the role of NR_4^+ cations is not indicated [Eqs. (3) and (13)–(15)]. d) Schematic representation of the initial dynamics for large fluxes of mediator radical anion, showing the occurrence of the two parallel mechanisms: reduction through electronic conduction in the *n*-doped carbonized zone [Eqs. (13)–(15)] and through direct reaction between the mediator radical anion and PTFE [Eq. (3)].

Experimental Section

Two series of ultramicroelectrode assemblies were constructed along the same "sandwich " technique[7] pictured in Figure 1. A gold foil (thickness: $w = 10$ µm, length: $l = 3$ mm, Goodfellow, 99.95%) was placed on a flat glass substrate, covered by a mylar insulating film (thickness: $g = 10$ µm) and then by a PTFE sheet a few millimeters wide (operating assembly). For the control assemblies (microband alone), the ensemble mylar–PTFE was replaced by a glass sheet. The whole sandwich was then firmly pressed into position and soaked onto an epoxy resin (Epon, type 828) mixed with 10% triethylene tetramine (Aldrich, technical grade). After hardening of the epoxy, the gold foil was connected to an electrical copper lead and the whole assembly was consolidated by a mechanically strong resin (Torr Seal, Varian) and glued inside a glass tube of 1 cm internal diameter. After hardening, the cross-section of the in-tube sandwich assembly, exposed with a diamond saw, displayed a gold microband ($w = 10$ µm, $l = 3$ mm) separated from the PTFE (operating assembly) material by the insulating mylar gap ($g = 10$ µm) or the microband alone (control assemblies). This cross-section was polished with a polishing wheel with thinner and thinner abrasives (P600, P2500, P4000) before each measurement. The actual dimensions (*w*,*g*,*l*) of each microband assembly were controlled by optical microscopy (Figure 1a). The dimensions of the gold microbands (*w*,*l*) were more precisely determined for each assembly by chronoamperometric calibrations following a previously described method[10, 11] that uses the one-electron reduction wave of 4-cyanopyridine, since its standard potential (−1.70 V vs. SCE) is not sufficiently negative to give rise to a reaction with PTFE (vide infra). In all cases the nominal thickness (*w*) was maintained and the lengths (*l*) were equal to 3 mm within ±5%. Since the current of a microband electrode assembly is strictly proportional[7–13] to the band length, all the currents reported here were post-normalized in each case to a 3 mm length to allow comparison between all assemblies.

The cell contained 15–20 mL of a solution of the mediator and of NR_4BF_4 (R = Et, *n*Bu, *n*Hex) supporting electrolyte in dry DMF. The solution was deaerated by argon bubbling and then maintained under an argon blanket. DMF (Carlo Erba, for analysis) was distilled from BaO to ensure a proper dryness, since most of the experiments were performed at rather negative potentials (generally −2.4 V vs. SCE) at which water traces give rise to significant residual currents. NBu_4BF_4 was synthesized and recrystallized according to a previously reported procedure.[14] The two other supporting electrolytes (NR_4BF_4, R = Et, *n*Hex, Fluka Chemie, purum) were used as received. All the mediators (phtalonitrile, 4-cyanopyridine, pyridazine, 4-phenyl-pyridine, benzonitrile, and naphthalene) examined in this study were commercial (puriss quality) and used without further purification.

A three-electrode configuration was used. The SCE reference electrode (Tacussel) was set into a bridge of a composition identical to that of the investigated solution and separated from the solution by a thin glass frit (Tacussel). The counter-electrode consisted of a platinum coil of approximately 1 cm^2 surface area. The working microband electrode potential was imposed and the currents measured by a Autolab integrated potentiostat driven by the Autolab GPES software run by a Pentium computer. Most experiments were performed chronoamperometrically, the electrode potential being poised on the plateau of the mediator reduction wave (most generally, about 130 mV more negative than its half-wave potential).

Most experiments required long duration times. We observed that when operated alone, the microband current (control device) remained rather

invariant with time in the range of interest, albeit for a pure diffusion transport it is expected to vary reciprocally with $\ln t$.[12, 13] This demonstrated that convection dominated the transport to the microband in the time range of interest. Furthermore, several experiments involved benzonitrile concentrations comparable with or even larger than that of the supporting electrolyte, that is, they were performed under conditions under which convection driven by electrophoretic density necessarily participated into the transport processes occurring in the solution.[15] For this reason, in all experiments, including those performed under an inverted microscope, the electrode was always placed with its horizontal active surface facing the bottom of the cell (at approximately, 5 mm from the cell bottom) and at the same position within the cell in order to maintain, as much as possible, reproducible convective conditions in different runs performed under otherwise identical conditions. For the same reason the cell (or the ensemble of the cell and microscope, vide infra) was always mounted on a vibration free table.

The optical measurements of the lateral growth (L) of the carbonized layer were made on the stage of an inverted microscope (Axiovert 135, Carl Zeiss) equipped with a charge-coupled device video camera (model VCB-3512P, Sanyo) connected to a black and white video monitor (model VM-2512, Sanyo), a tape recorder (Panasonic), and a video graphic printer (Sony). The photographs shown in Figure 1 (see also Figure 7 later) were recorded and printed this way. The microband/mylar/PTFE assemblies were set in position with a three-dimensional manipulator and mounted with their active surface facing the cell bottom and exposed to the microscope lens ($\times 20$). The magnification (2 mm on original printed views corresponded to 10 μm) was chosen so that it had not to be changed during the full duration of an experiment, while the full lateral development of the carbonized zone could be observed. The microscopic field was lighted with a cold-light source equipped with an optical-fiber light-transmission device (KL 1500 electronic, Schott). The cell was a sectioned beaker bottom (55 mm diameter, 4 cm height) filled with 20 mL of a DMF/supporting electrolyte (NEt_4BF_4, 0.2 M in the experiments shown in this work) solution of the mediator. The chronoamperometric electrochemical experiments were performed as described above. The current was recorded as a function of time, while the microscopic image was simultaneously recorded on the tape recorder. For the treatment of the lateral growth (L), the video recorder internal clock was used in retrieving the $L(t)$ variations. To ensure that no drift occurred between the two timescales (namely, that of the Autolab potentiostat for the current and that of the video recorder for the length) over the long durations of the recordings, some of the pictures were marked electronically during their recording at selected times imposed by the Autolab timescale. The measurements of $L(t)$ values were performed from the views printed at selected times with a ± 0.25 mm accuracy (that is a ± 1.25 μm accuracy on L values). The optical measurements of microband (w) and gap (g) widths were performed similarly by using a better adapted magnification, since that used in Figures 1a and 7 was too small to obtain the required precision. Similarly, the contrast and cold-light angle in Figures 1a and 7 were adjusted to allow the best examination of the carbonized zone, but resulted improper for a precise determination of w and g because of the ensuing shadows.

Principle and Theory

Figure 1a,b shows in schematic form the principle of the experiments performed in this study. The mediator M is reduced at the gold microband surface so that the generated radical anion $M^{\bullet -}$ diffuses cylindrically in the solution.[12, 13] For the gap width used here, a few seconds are sufficient for the cylindrical diffusion "layer" to extend over the insulating gap so as to reach the PTFE edge. $M^{\bullet -}$ may then react electrochemically with the PTFE carbon–fluorine bonds in a way reminiscent to redox catalysis.[16] Indeed, based on previous reports,[5, 6] one expects to observe the regeneration of the unreduced M form through the overall reduction [Eqs. (1) and (2)] taking place at the PTFE/solution interface.

Albeit for different physicochemical reasons, the whole assembly is then expected to act as a generator–collector two band assembly.[7–9, 13] The redox catalytic reaction [Eq. (3)] indeed performs in a way such that the PTFE behaves as a collector.

$$-(CF_2)_n- + (2+\delta)n\,M^{\bullet -} + (2+\delta)n\,NR_4^+ \longrightarrow [-(C^{\delta -})_n-,\delta n\,NR_4^+] + 2n\,[NR_4^+,F^-] + (2+\delta)n\,M \quad (3)$$

Whenever the maximum allowable rate of the reaction [Eq. (3)] is faster than the flux of incoming radical anion, the feedback due to the mediator regeneration is expected to be total. Thus, the total microband current (I) must be larger than for the same band operating in the absence of adjacent PTFE (I_{band}).[7–9, 13] The current amplification (namely, I/I_{band}[7, 13]) must then be identical to that of a generator–collector assembly with identical band and gap widths and with the collector potential set on the plateau of the oxidation wave of the reduced mediator. Conversely, when the reaction [Eq. (3)] is rate determining, a less efficient regeneration is expected to occur (vide infra), and therefore the current amplification is expected to be much less than that of a true generator–collector assembly. Hence, the measured values of I/I_{band} or of the catalytic current $I_{cat} = I - I_{band}$ appear to be suitable and quantitative indicators of the rate of reaction [Eq. (3)] under the present circumstances.

Although its general conclusions are right qualitatively, this simple view neglects the electrochemical role of the altered PTFE zone formed by the reduction in Equation (3), and is therefore [Eq. (3)] strictly valid only for short times. In truth, the reaction removes the reducible carbon–fluorine bonds adjacent to the immediate gap edge regions, and the resulting n-doped carbonized material may then convey the current flux to its internal boundary with the unaltered PTFE. The process then becomes more complex when the flux of reduced mediator is high and a significant length (L) of the PTFE surface has been altered, that is, when L is no longer negligible in relation to g. Under such conditions, different kinetic situations must be considered depending on the resistivity of the carbonized region and on the diffusivity of NR_4^+ and F^- ions in this zone with regard to the flux of the reduced mediator generated at the microband and the overall rate of the process in Equation (3).

Preliminary considerations: From what precedes it is understood that the dynamic behavior of the system is controlled by two main phenomena. One is the internal transport dynamics and kinetics occurring in the carbonized area and the other is the solution transport dynamics. Both are crucial as is established in the following analysis. Since they are documented only disparately in the literature and not at all in this particular context, it is important to briefly review and implement them in this preliminary section. This will ease the development of the parts that are the true original core of the present theoretical section and which will be developed after these preliminary considerations.

Diffusion at microbands and generator–collector microband assemblies:[7–13] A microband may perform under two differ-

0947-6539/00/0605-0822 $ 17.50+.50/0 *Chem. Eur. J.* **2000**, *6*, No. 5

ent diffusional regimes according to the timescale. The occurrence of these two regimes is controlled by the size of the microband width (w) relative to that of the diffusion length, $(Dt)^{1/2}$, where t is the duration of the experiment and D the diffusion coefficient of the electroactive species present at concentration c_M in solution. Thus, when $\underline{p} = (w/2)(Dt)^{-1/2}$ is much larger than unity, the diffusion layer is a thin film adjacent to the electrode surface and of negligible width relative to the microband width, so that diffusion is mostly planar. The microband current is then given by a classical Cottrell equation.[17] Conversely, when $\underline{p} \ll 1$, the diffusion length is extremely large with regard to w and a hemicylindrical diffusion layer centered on the microband axis develops.[12, 13] Under these long time conditions, the diffusion occurs under a quasi-steady-state regime, and the microband current for chronoamperometry on the electroactive species plateau is given by Equation (4), in which l is the microband length ($l \gg w$), $\Delta_{diff}/w = (1/\pi)\ln(4/\underline{p}) = (1/\pi)\ln[8(Dt)^{1/2}/w]$, F = 96485, and n is the number of electrons exchanged in the electrochemical reaction (note the "minus" sign in Equation (4), since $n > 0$ for a reduction, while cathodic currents are negative by convention).[12, 13]

$$-I_{band} = nFDlc_M(w/\Delta_{diff}) \quad (4)$$

Equation (4), predicts a slow logarithmic decay of the microband current with the operation time, reflecting the slow logarithmic expansion of the hemicylindrical diffusion layer. This remains true provided that the hemicylindrical diffusion layer is small enough to remain included within the convection-free layer adjacent to the plane in which the microband is embedded.[13] When this condition is not fulfilled, convection limits the extension of the diffusion layer and the microband current is then defined by Equation (5)[18], in which Δ_{conv} is an effective length determined by the thickness δ_{conv} of the convection-free layer (see ref. [19] for a treatment in the case of a disk electrode). This convective transport becomes dominant when $\underline{p} \leq \underline{p}_{conv} = 4\exp(-\pi\Delta_{conv}/w)$.

$$-I_{band} = nFDlc_M(w/\Delta_{conv}) \quad (5)$$

Let us now consider a generator–collector microband assembly formed of two parallel microbands of identical widths (w) and lengths (l), separated by an insulating gap of width g, embedded in an insulating plane. At time zero of the experiment the generator electrode potential is set at the plateau of the electroactive substrate, and that of the collector set at the plateau of the reverse electrochemical reaction. Based on the above, four regimes will be successively met with when the time t increases. When $\underline{p} = (w/2)(Dt)^{-1/2} \gg 1$, the diffusion layer forming at the generator is planar and confined over the generator surface. The generator current is given by the Cottrell equation, and the collector current is zero. Over the interval $1 \geq \underline{p} \geq \underline{p}_{conv}$, two different situations are observed depending on the respective size of the gap and the diffusion length, that is, depending on the value of the parameter $p = (g/2)(Dt)^{-1/2}$.[7, 13]

When $p \gg 1$, the diffusion length is too small for the species electrogenerated at the generator to reach the collector. Thus the collector current remains zero and the generator microband behaves as if it was alone: its diffusion layer is hemicylindrical and its current is given by Equation (4). Note that since $p = (g/w)\underline{p}$, this situation is not observed experimentally when $g \ll w$. Conversely, when $p \ll 1$, a complete diffusional cross-talk occurs between the two microbands[7–9, 13] so that all the species electrogenerated at the generator are converted back to the electroactive substrate at the collector. The collection efficiency is unity, and the whole dynamics of the assembly is regulated by this cross-talk. The generator and collector currents are identical and given by Equation (6) (the superscript ∞ indicates that the value corresponds to infinite times), in which $\vartheta_{w/g}$ is given by the ratio of elliptic integrals [Eq. (7)];[7, 13] this depends only on w/g and is readily evaluated numerically (see Figure 4 in ref. [7])

$$I_{gen} = -I_{coll} = I^{\infty} = -nFDlc_M\vartheta_{w/g} \quad (6)$$

$$\vartheta_{w/g} = \tfrac{1}{2}\frac{\int_1^{1+2w/g}\{(\zeta^2-1)[(1+2w/g)^2-\zeta^2]\}^{-1/2}d\zeta}{\int_0^1\{(1-\zeta^2)[(1+2w/g)^2-\zeta^2]\}^{-1/2}d\zeta} = \tfrac{1}{2}\frac{\int_1^{\mathrm{Ar\,cosh}(1+2w/g)}[(1+2w/g)^2-(\cosh w)^2]^{-1/2}dw}{\int_0^{\pi/2}[(1+2w/g)^2-(\sin w)^2]\}^{-1/2}dw} \quad (7)$$

Note that under those conditions $I_{band} \to 0$ when convection is negligible (namely, for $\Delta_{conv} \gg w$), since $\underline{p}$ is very small, so that $I/I_{band} \propto -\ln(\underline{p}) \to \infty$. In the intermediate zone, that is, when p is of the order of unity, the collection is not quantitative (see Figure 7B in ref. [7]) so that the generator microband current and the collection efficiency increase, while the time increases. A convenient approximation of the generator microband current is then given by Equation (8), in which I_{band} is given in Equation (4) and the function $\Phi(p)$ is shown in Figure 2a and is obtained by combination of Figures 5 and 7B in ref. [7].

$$I_{gen}/I_{band} - 1 = \vartheta_{w/g}\Phi(p) \quad (8)$$

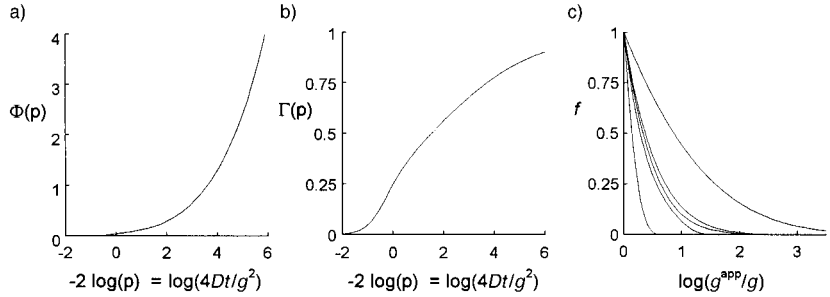

Figure 2. Theoretical variations of the functions a) $\Phi(p)$ and b) $\Gamma(p)$ with p and t. c) Theoretical variations of the function $f(g^{app}/g)$ at constant $p = g/[2(Dt)^{1/2}]$ value (see text); from top to bottom, $\log(p) = -\infty, -3, -2, -1$, and 0. Under our conditions, $-3 \leq p \leq -1$.

When the time increases, I_{gen}/I_{band} increases because $\Phi(p) \propto -\ln(p)$ when the time is large (Figure 2a). Again, this increase reflects mostly the decrease of I_{band}, since I_{gen} tends towards its limit I^{∞}, given in Equation (6). This continuous rise of I_{gen}/I_{band} with t is pursued up to the point at which Δ_{diff} becomes comparable with Δ_{conv}, that is, up to when $\underline{p} \leq 4\exp(-\pi\Delta_{conv}/w)$. The convection-limited behavior is then reached for operation times that exceed $t_{lim} = [(w/8)^2 \exp(2\pi\Delta_{conv}/w)]/D$.

To the best of our knowledge the situation in which convection interferes drastically has never been investigated theoretically for double-band assemblies. However, one may propose a simple approach of the phenomenon at hand. For micrometric values of w and g, this situation occurs when $\underline{p}$ and p are extremely small, that is, when the collection efficiency of the collector electrode is quantitative in the absence of convection. Thus, based on the above I_{gen} is given by Equation (9), in which I_{band} is the microband current [i.e., when the collector is disconnected, Eq. (5)] recorded under the same conditions, and Ω is the effective collection efficiency in the presence of convection.

$$I_{gen} \approx I_{band} + I_{p\to 0}\,\Omega = I_{band} - nFDlc_M\,\vartheta_{w/g}\,\Omega \quad (9)$$

Ω may be approximated by considering that the collection efficiencies of the collector and of the bulk solution are proportional to the diffusional gradients they create in cross-talking with the generator, that is, they are reciprocal to their apparent diffusion lengths from the generator. For the convection layer, the apparent diffusion length is Δ_{conv}, based on the formulation of I_{band} in Equation (5). For the collector microband, the apparent diffusion length is approximately $\pi g/2$ as previously evaluated (see the empirical Equation (17) in ref.[7]), thus $\Omega \approx \Delta_{conv}/(\Delta_{conv} + \pi g/2) = 1/(1 + \pi g/2\Delta_{conv})$, in which Δ_{conv} may be determined from the current of the microband operating alone [Eq. (5)].

From I_{band} in Equation (5), Equation (10) can be derived. Note that Equation (10) is the same as Equation (8) in which

$$I_{gen}/I_{band} - 1 \approx \vartheta_{w/g}(\Delta_{conv}/w)\,\Omega \quad (10)$$

$\Phi(p)$ is replaced by $(\Delta_{conv}/w)\Omega$. In other words, this means that when the time increases to infinity, $\Phi(p)$ does not rise to infinity as it would for a pure diffusive transport, but instead reaches a limit at $(\Delta_{conv}/w)\,\Omega$ because of convection. Interestingly this number can be readily evaluated from the experimental microband current alone, since this affords Δ_{conv} (compare [Eq. (5)]).

Electrochemical kinetics in the PTFE bulk: Since the carbonized PTFE is *n*-doped, it may act as an electronic conductor able to shuttle the electrons delivered by the oxidation of the reduced mediator at the carbonized PTFE/solution interface inside the core of the material, where they can be used to reduce CF_2 groups of the unaltered PTFE in contact with the carbonized zone. Such a reduction is coupled with the diffusion–migration of F^- and NR_4^+ ions in the carbonized matrix to and from the PTFE/solution interface, respectively. So the situation is identical to that which occurs in an electrochemical cell, and v, the overall carbonization rate defined as the moles of CF_2 groups reduced per unit of time and unit of surface area, must follow Equation (11),[17] in which j^{diff} is the maximum current density allowed by the diffusion–migration of NR_4^+ and F^- within the carbonized zone[17, 20–22], k is the heterogeneous rate constant (in units of $cm\,s^{-1}$)[17] of the reduction at the interface between PTFE and carbonized PTFE, and $c = 44$ M is the concentration of CF_2 groups in PTFE.

$$1/[(2+\delta)Fv] \approx 1/j^{diff} + 1/[kc(2+\delta)F] \quad (11)$$

When k is large enough with regard to j^{diff}, Equation (11) shows that $(2+\delta)Fv \approx j^{diff}$ so that the process is controlled mostly by diffusion–migration of ions in the carbonized matrix. In this case it is essential to compare the lateral and vertical progressions of the carbonized zone. For the sake of simplicity let us consider a parallelepipedic carbonized zone of lateral extension L and depth h as sketched in Figure 3a (note that this reasoning is directly transposable to any shape

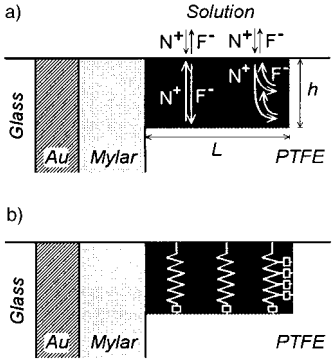

Figure 3. a) Schematic representation of the diffusion–migration dynamics in the carbonized PTFE (N^+ represents the NR_4^+ ion). b) Schematic electrical equivalent of the carbonized PTFE region and of its interface with PTFE. The boxes located at the interface represent the Faradaic impedance placed in parallel with the double layer capacitance of the interface.[23] Note that for the lateral Faradaic reactions, the Faradaic impedances are connected in parallel on the vertical resistance, while for the bottom Faradaic reactions, they are connected in series with the same vertical resistance.

through considering finite volume elements, $l\mathrm{d}h\mathrm{d}L$ followed by integration). A vertical progression forces the F^- and NR_4^+ ions to move over the distance h. Then j^{diff} conforms to the diffusion–migration laws,[17] so that if the current supply at the solution interface is constant, one has $v_h \approx (j^{diff})_h/[(2+\delta)F] \propto (\kappa_h t)^{-1/2}$, in which κ_h is an apparent diffusion coefficient.[17, 20–22] For the lateral progression, the points of reduction involve different diffusion–migration lengths, since they are located at variable distance from the solution: the top of the interface is in contact with the solution (namely, $(j^{diff})_L \approx \infty$), while its bottom is at distance h (namely, $(j^{diff})_L \approx (j^{diff})_h$) (Figure 3a). Thus, $v_L \approx \langle (j^{diff})_L \rangle/[(2+\delta)F]$, in which $\langle (j^{diff})_L \rangle$ is the mean value of $(j^{diff})_L$ over the segment $[0,h]$, is larger than v_h. It follows that when the current supply at the solution interface is constant, that is, $v_L \propto (\kappa_L t)^{-1/2}$ in which κ_L is again an apparent diffusion coefficient and $\kappa_L > \kappa_h$. This simple reasoning shows that under a pure diffusion–migration control and a constant reductive flux at the solution interface,

0947-6539/00/0605-0824 $ 17.50+.50/0 *Chem. Eur. J.* **2000**, *6*, No. 5

the carbonized zone progresses in a diffusion-like fashion, though with different vertical and lateral apparent diffusion coefficients. Yet, $L/h = (\kappa_L/\kappa_h)^{1/2}$ so that its cross-section is an elliptic quadrant with a constant ellipticity as a function of time.

In the converse situation, that is when k is small with regard to j^{diff}, Equation (11) gives $v \approx kc$, so the overall rate of reduction is controlled by the heterogeneous electron transfer at the carbonized PTFE/PTFE interface. The diffusion–migration performs under steady state so that the overall current I^{PTFE} entering the carbonized zone through oxidation of the mediator radical anion is equal to the integral of $(2+\delta)Fv$ over the surface area of the interface between the carbonized zone and the unaltered PTFE. Thus I^{PTFE} is given by Equation (12) (note that I^{PTFE} is negative since it is a cathodic

$$-I^{PTFE} = (2+\delta)Flc\int_{\mathscr{P}} k_{\mathscr{P}}\,d\mathscr{P} = \rho(2+\delta)Flc\,[k^L_{av}h + k^h_{av}L] \qquad (12)$$

current; hereafter it will be noted $I_{band} - I$), in which $\mathscr{P}$ is the curvilinear length of the cross-section carbonized PTFE/PTFE interface, and $k_{\mathscr{P}}$ is the value of k at the considered point $\mathscr{P}$ of the interface. ρ is a shape factor whose value depends on the shape of the cross-section of the carbonized zone ($\rho = \pi/4$ for an elliptic quadrant, vide infra). k^L_{av} and k^h_{av} are the average values of $k_{\mathscr{P}}$ over the lateral interface (whose length is h) or over the bottom interface (whose length is L), respectively. As before, it is interesting to remark that $L/h = k^L_{av}/k^h_{av}$ is independent of time whenever k^L_{av}/k^h_{av} does not vary significantly, even if each rate constant varies. Under these circumstances, the cross-section of the carbonized zone is again an elliptic quadrant of half-axis L and h, though now the ellipticity may differ from that in the previous case.

Formally, one would expect that $k^L_{av} \approx k^h_{av}$, because the two constants feature the same reductive process. However, as $k_{\mathscr{P}}$ is a rate of electron transfer, it has to depend on the locally available reductive driving force,[17] which necessarily decreases when the carbonized zone penetrates deeper and deeper into the PTFE bulk because of the increasing ohmic drop. In this respect, it is worth mentioning that a decrease of only approximately 130 mV in reductive strength of the mediator is enough to impede drastically the rate of carbonization (vide infra). Whenever ohmic drop and accumulation of defects are significant, one expects that both rate constants will decrease with time. It is important to note that the surface of the carbonized zone is in contact with the solution that contains the redox mediator. This allows a back and forth electron exchange between the reducing carbonized material and the solution. Therefore, in a first-approximation level, the system is equivalent to those examined previously in the context of artificial neurons,[10, 11] with the result that one may consider that the surface of the carbonized zone exposed to the solution is approximately one equipotential surface, even when the ohmic drop in the bulk carbonized zone is not negligible. Based on this important observation, the same reasoning as developed above shows that provided that L is not too large, the ohmic drop relative to the lateral expansion (namely, controlling k^L_{av}) is smaller than that relative to the vertical expansion (namely, controlling k^h_{av}). Indeed, its value is an average between zero (part of interface in contact with the solution) and that relative to the vertical expansion (Figure 3b). Then, whenever ohmic drop plays a significant role, k^h_{av} is expected to be smaller than k^L_{av}, and both are expected to decay with time because h increases.

Based on these considerations, one predicts that for a given current supplied to the PTFE carbonized zone by means of oxidation of an homogeneous reducer $M^{\bullet -}$ generated at the microband, two different kinetic regimes may control the expansion of the carbonized zone depending on the magnitude of the microband current intensity. For a given generator microband, whose potential is set at the plateau of the mediator reduction wave, this intensity is fixed only by the concentration c_M of the mediator. In the following we wish thus to address these two different kinetic regimes separately.

Small reducing fluxes: At low current fluxes the electrochemical kinetics at the interface between the carbonized region and PTFE does not limit the kinetics. Thus, while the PTFE surface is reduced, it acts as a metallic collector of a progressively enlarging length (L) and thickness (h), and the overall device is expected to perform as those we investigated previously in the context of artificial neurons.[10, 11] Under these circumstances, the mediator is to be regenerated mostly over a limited area located at the edge of the carbonized PTFE and in contact with the insulating gap ($0 \le L \le L_0$, with $L_0 \approx$ g) because of the infinite current densities at conductor edges in double-band assemblies.[7, 11, 13] The electrons thus released at this point in the PTFE carbonized region by oxidation of the mediator radical anion are shuttled to the interface between the carbonized region and the still unaltered PTFE, where it is used to reduce new carbon–fluorine bonds. The carbonized region should then expand laterally (L) and vertically (h) in a diffusion-like fashion (vide supra). This is summarized in Figure 1c and in Equations (13)–(15),

solution edge of carbonized PTFE (adjacent to the insulating gap):[7–11, 13]

$$(2+\delta)n\,M^{\bullet -} \longrightarrow (2+\delta)n\,M + (2+\delta)n\underline{e} \qquad (13)$$

interface between carbonized PTFE and unaltered PTFE:[1–6]

$$2n\underline{e} + -(CF_2)_n- + 2n\,NR_4^+ \longrightarrow -(C)_n- + 2n[NR_4^+,F^-] \quad \text{(fastest)} \qquad (14)$$

$$\delta n\underline{e} + -(C)_n- + \delta n\,NR_4^+ \longrightarrow [-(C^{\delta -})_n-,\delta n\,NR_4^+] \quad \text{(slowest)} \qquad (15)$$

in which the notation $\underline{e}$ represents an electron in the conduction band of the PTFE carbonized matrix. Note that the combination of Equations (13)–(15) is strictly equivalent to that of Equations (1) and (2) or to Equation (3) except that we consider now that they occur at different locations of the system.

The system is then expected to behave strictly as a generator–collector double band[7–11, 13] of identical width, so that the variations of its current with time are given by Equations (8) or (10), depending on the magnitude of Δ_{conv}, and Equation (16) can be defined.

$$I/I_{band} - 1 = \vartheta_{w/g}\,\Phi^*(p) \qquad (16)$$

In Equation (16) $\Phi^*(p) = \Phi(p)$ for $\Phi(p) \le (\Delta_{conv}/w)\Omega$, or $\Phi^*(p) = (\Delta_{conv}/w)\Omega$ in the converse situation. Thus, I/I_{band} is expected to rise smoothly from unity at short times (where no feedback occurs) to a constant value $1 + \vartheta_{w/g}(\Delta_{conv}/w)\Omega$ at long times (where total convection-controlled feedback occurs). This constant value is achieved for $t \ge t_{lim} = [(w/8)^2 \exp(2\pi\Delta_{conv}/w)]/D$, that is, in conjunction with the achievement of the steady state convection-limited current by the microband alone. For the geometrical arrangement used in this study this is expected to occur after operating the system for a few tens of seconds.[13, 23, 24]

When this convective steady state behavior is reached, the currents I^{PTFE} and I_{band} are constant so that the charge $Q^{PTFE}(t)$ used for carbonization, that is, that corresponding to the time integration of $I^{PTFE} = I - I_{band}$, increases linearly with the operation time. Whenever δ is constant the volume of carbonized PTFE (proportional to Lhl) matches the variations of Q^{PTFE}. Thus, the product hL must also vary linearly with the time, which agrees with the above prediction that $h \propto t^{1/2}$ and $L \propto t^{1/2}$.

Large reducing fluxes: When the maximum current sustainable by the carbonized zone is too small with regard to the flux of reduced mediator emitted by the microband, only a fraction of the reduced mediator generated at the microband can be oxidized at the edge of the carbonized zone touching the insulating gap (namely, at a distance g of the band edge). The unoxidized fraction diffuses in the solution and, provided that the solution diffusion layer is larger than L, it may reach unreduced PTFE where it can be oxidized (Figure 1d). This fraction is then oxidized beyond an apparent gap $g^{app} = g + L(t)$, which increases with time as $L(t)$. Initially, $L(t) \ll g$ so that $g^{app} \approx g$. Therefore at short times the initial amplification current is the same as in the low current regime (Figure 1c) although the two mechanistic situations are extremely different. Conversely, when $L(t)$ increases, $\vartheta(p^{app})/\vartheta(p)$ (in which $p^{app} = (g^{app}/2)(Dt)^{-1/2}$) decreases drastically, so that the solution by-pass contributes less and less to the cross-talk with the generator microband.

Overall, I/I_{band} is then expected to rise at initially, while the diffusional cross-talk is progressively established over the gap g (that is over the first few tens of seconds of operation for our present assemblies[13, 23, 24]) and then decrease with time to reach eventually a limit imposed by the kinetics of the reduction at the PTFE/carbonized PTFE interface when the solution by-pass becomes negligible. Yet, when L and h increase, the surface area of the PTFE/carbonized PTFE interface increases, so that v increases whenever k^L_{av} and k^h_{av} retain their initial values. So, after a certain amount of time the overall kinetic current I^{PTFE} is expected to increase again [see Eq. (12)]. Eventually, the surface area of the interface may become large enough to sustain a current that is comparable with the maximum one supplied by the reduced mediator at g. At this point the system shifts to a low-flux mode and $(I/I_{band} - 1) \to \vartheta_{w/g}(\Delta_{conv}/w)\Omega$. Yet, when the flux of mediator is large enough, occurrence of this situation may require a too large extension of the interface surface area, so that other effects (ohmic drop, defects, etc.) may dominate and limit the current before this situation may be observed.

Based on the conformal mapping formalism developed previously[7, 13] the resulting current I is given by the sum of the current I_{band} of the microband operating alone, with the two catalytic currents $I^{PTFE}(g)$ and $I^{PTFE}(g^{app})$ due to each fraction of the mediator regenerated at g and at $g^{app} = g + L(t)$. Thus Equation (17) can be defined.

$$I/I_{band} - 1 = I^{PTFE}(g)/I_{band} + I^{PTFE}(g^{app})/I_{band} \quad (17)$$

Taking η to be the fraction oxidized at g and $(1 - \eta)$ that at g^{app}, one has then $I^{PTFE}(g)/I_{band} = \eta[(I/I_{band})_{w,g} - 1]$ and $I^{PTFE}(g^{app})/I_{band} = (1 - \eta)[(I/I_{band})_{w,g^{app}} - 1]$, in which $(I/I_{band})_{w,G}$ is the amplification factor for a generator–collector assembly with a generator of width w and an insulating gap of thickness $G = g$ or g^{app} for the considered value of $\Phi^*(p)$ or $\Phi^*(p^{app})$, respectively [Eq. (16)]. On the other hand, the catalytic current at g is limited by the maximum rate (noted V_{max}, vide infra) of the heterogeneous reduction through the carbonized layer, and by the collection efficiency $\Gamma(p)$ shown in Figure 2b.[7] While p decreases, $\Gamma(p)$ increases from zero to Ω, its limit imposed by convection. Then $I^{PTFE}(g)/I_{band}$ is given by Equation (18), which affords the value of η. This allows the rewriting of Equation (17) to give Equation (19) in which $f = [(I/I_{band})_{w,g^{app}} - 1]/[(I/I_{band})_{w,g} - 1]$ and $(I/I_{band})_{w,g}$ is given by Equation (16).

$$I^{PTFE}(g)/I_{band} = \eta[(I/I_{band})_{w,g} - 1] \approx [(2 + \delta)FlV_{max}/(I_{band})]\Gamma(p) \quad (18)$$

$$I/I_{band} - 1 = [(2 + \delta)FlV_{max}/(I_{band})]\Gamma(p)(1 - f) + [(I/I_{band})_{w,g} - 1]f \quad (19)$$

Equation (19) can then be rewritten as Equation (20), in which f is given by Equation (21). At infinite times, $g^{app} \gg g$ and $f \to 0$ because $(\vartheta_{w/g^{app}}/\vartheta_{w/g}) \to 0$[7] and $[\Phi^*(p^{app})/\Phi^*(p)] < 1$. Since $\Phi^*(p)$ is by definition smaller than or equal to $(\Delta_{conv}/w)\Omega$, and $\Gamma(p) \to \Omega$ under convective conditions, Equation (20) simplifies into Equation (22) [note that Eq. (5) is used for I_{band}, since this features the convective limit of I_{band}].

$$I/I_{band} - 1 = (1 - f)[(2 + \delta)FlV_{max}/(I_{band})]\Gamma(p) + f\vartheta_{w/g}\Phi^*(p) \quad (20)$$

$$f = (\vartheta_{w/g^{app}}/\vartheta_{w/g})[\Phi^*(p^{app})/\Phi^*(p)] \quad (21)$$

$$(I/I_{band} - 1) \to [(I/I_{band})^{\infty} - 1] = [(2 + \delta)V_{max}/(nDc_M)](\Omega\Delta_{conv}/w) \quad (22)$$

Equation (22) shows that in agreement with our above intuitive reasoning, the carbonization then proceeds only by the kinetically limited sequence in Equations (13)–(15) because g^{app} is then too large for the solution–diffusion pathway to contribute significantly to the current. Conversely at short times, $g^{app} \approx g$ so that $f \approx 1$ and Equation (20) simplifies into Equation (23), which shows that in agreement with our above intuitive reasoning, the initial current tends to be the same as if the system was operating as a generator–collector of gap g, that is, it acts as if there was no kinetic limitation due to Equations (13)–(15) because the solution–diffusion pathway by-passes the heterogeneous kinetic limitations.

Since $(I/I_{band})^{\infty}$ and $(I/I_{band})^0$ defined in Equations (22) and (23) are readily available experimentally or theoretically,

0947-6539/00/0605-0826 $ 17.50+.50/0 Chem. Eur. J. 2000, 6, No. 5

Equation (20) is best formulated as in Equation (24), in which $\gamma(\mathrm{p}) \approx \Gamma(\mathrm{p})\Delta_{\mathrm{diff}}/(\Omega\Delta_{\mathrm{conv}}) \approx \Phi(\mathrm{p})\,\Omega(w/\Delta_{\mathrm{conv}})$ when convection is negligible,[7] and $\gamma = 1$ in the converse situation [compare with Eqs. (4) and (5)].

$$(I/I_{\mathrm{band}} - 1) \rightarrow [(I/I_{\mathrm{band}})^0 - 1] = \vartheta_{w/g}\,\Phi^*(\mathrm{p}) \quad (23)$$

$$I/I_{\mathrm{band}} - 1 = [(I/I_{\mathrm{band}})^\infty - 1]\,\gamma(\mathrm{p}) + f\{\vartheta_{w/g}\,\Phi^*(\mathrm{p}) - [(I/I_{\mathrm{band}})^\infty - 1]\,\gamma(\mathrm{p})\} \quad (24)$$

Thus $\gamma(\mathrm{p}) \approx \Phi^*(\mathrm{p})\,\Omega(w/\Delta_{\mathrm{conv}})$. This equation shows that the current is formed of two components of essentially different physicochemical origins. The first term, proportional to $\Phi^*(\mathrm{p})$, smoothly varies from zero at short time to $[(I/I_{\mathrm{band}})^\infty - 1]$ [Eq. (22)] at long times. It essentially features the establishment of the cross-talk between the generator microband and the carbonized zone, which acts as a kinetically-saturated collector located at a constant distance g from the microband. Because of the kinetic saturation, when the concentration of the mediator increases, this component has a smaller and smaller amplitude relative to $I_{\mathrm{band}} \propto c_{\mathrm{M}}$: $[(I/I_{\mathrm{band}})^\infty - 1] \propto (1/c_{\mathrm{M}})$.

The second term represents the effect of the solution–diffusion pathway. At moderate operation times and large mediator concentrations, it has a much larger magnitude than the first one. This term results from the convolution of two factors that follow opposite trends. On the one hand, f decays with time [Eq. (21)] from unity to zero and is mostly influenced by the increase of g^{app}/g with time (see Figure 2c). Indeed, the ratio $\Phi^*(\mathrm{p}^{\mathrm{app}})/\Phi^*(\mathrm{p})$ is not influenced at all by t at short times, because then $\mathrm{p}^{\mathrm{app}} \approx \mathrm{p}$, and it is only modestly affected (namely, in a logarithmic fashion[7]) by t at long times. On the other hand, the multiplier of f in Equation (24) is a component that increases with time, being zero initially and tending towards a convection-bound limit, $\Omega(\Delta_{\mathrm{conv}}/w)\vartheta_{w/g} + 1 - (I/I_{\mathrm{band}})^\infty$, at long times at which p is small enough (Figures 2a and 2b). It is thus easily understood that the solution–diffusion term is zero at both short and long times, and therefore must pass through a maximum as the time evolves. The precise position and height of this maximum is difficult to evaluate quantitatively because of the intimate convolution between f and its multiplier.

This maximum can however be approximated by noting that the decay of f and the rise of its multiplier occur on different timescales. Indeed, the increase of the multiplier is controlled by p, which reflects the progressive establishment of the diffusional cross-talk over the insulating gap g. So in the small time range at which values p are too large for any significant cross-talk to be established, $g^{\mathrm{app}} \approx \mathrm{g}$ and thus $f \approx 1$. Conversely, whenever g^{app}/g is sufficiently large to affect f significantly (Figure 2c) p takes small values so that the multiplier of f almost reaches its infinite-time limit. Based on this difference between the two timescales, one may safely approximate that the maximum of the second term in Equation (24) is of the order of $(\Omega\Delta_{\mathrm{conv}}/w)\vartheta_{w/g} + 1 - (I/I_{\mathrm{band}})^\infty$. It occurs at $t \approx t_{\max}$ when Φ^* has reached its convection-imposed limit, namely, $\Phi^*[\mathrm{p}(t_{\max})] \approx \Omega(\Delta_{\mathrm{conv}}/w)$. Therefore, Equation (24) may be simplified so that it takes the much simpler forms [Eqs. (25) and (26)] before and after its maximum, with $\varphi + 1$ derived in Equation (27) from $\varphi + 1 = [(I/I_{\mathrm{band}})^0 - 1]/[(I/I_{\mathrm{band}})^\infty - 1] = \vartheta_{w/g}\,\Omega(\Delta_{\mathrm{conv}}/w)/[(I/I_{\mathrm{band}})^\infty - 1]$.

$$0 \le t < t_{\max}: \qquad I/I_{\mathrm{band}} - 1 \approx \vartheta_{w/g}\,\Phi^*(\mathrm{p}) \quad (25)$$

$$t > t_{\max}: \qquad I/I_{\mathrm{band}} - 1 \approx \vartheta_{w/g}\,\Omega(\Delta_{\mathrm{conv}}/w)\,[(1 + \varphi f)/(1 + \varphi)] \quad (26)$$

$$\varphi + 1 = nDc_{\mathrm{M}}\vartheta_{w/g}/[(2 + \delta)V_{\max}] \propto c_{\mathrm{M}} \quad (27)$$

Note that by the definition of the large flux regime $[(I/I_{\mathrm{band}})^0 - 1] \ge [(I/I_{\mathrm{band}})^\infty - 1]$, so that $\varphi + 1 \ge 1$. This condition simply expresses that $V_{\max} \le nDc_{\mathrm{M}}\vartheta_{w/g}/(2 + \delta)$. Since the surface area of the PTFE/carbonized PTFE interface increases as the time increases, $V_{\max}$ also increases provided that the heterogeneous rate constants retain their values. Thus, $\varphi + 1 \rightarrow 1$ and $I/I_{\mathrm{band}} - 1 \rightarrow \vartheta_{w/g}\,\Omega(\Delta_{\mathrm{conv}}/w)$ at infinite time (vide infra), which expresses simply that the system progressively shifts towards a low-flux regime when the extension of the carbonized zone is sufficient.

In summary, the rising branch ($t \le t_{\max}$) of the current is essentially the same as that observed for the low-current regime, while at longer times ($t \ge t_{\max}$) the carbonization current is composed of two contributions, so that $I = I_{\mathrm{band}} + I^{\mathrm{PTFE}}(g) + I^{\mathrm{PTFE}}(g^{\mathrm{app}})$. One contribution, $I^{\mathrm{PTFE}}(g)/I_{\mathrm{band}} = (\vartheta_{w/g}\Omega\Delta_{\mathrm{conv}}/w)/(1 + \varphi)$, represents that of the PTFE reduction proceeding through the electronic conduction in the carbonized PTFE. Since $(\varphi + 1) \propto c_{\mathrm{M}}$ [Eq. (27)] when the concentration of the mediator is made larger and larger, this contribution tends to become negligible relative to the microband current.

The other catalytic contribution, $I^{\mathrm{PTFE}}(g^{\mathrm{app}})/I_{\mathrm{band}} = \varphi f I^{\mathrm{PTFE}}(g)/I_{\mathrm{band}} = f[\varphi/(1 + \varphi)][\vartheta_{w/g}\Omega\Delta_{\mathrm{conv}}/w]$, is due to the solution–diffusion by-pass. It decays from $\varphi\, I^{\mathrm{PTFE}}(g)/I_{\mathrm{band}}$ at $t_{\max}$, to zero when the time increases much beyond $t_{\max}$; its time variations feature are essentially those of f [Eq. (21)]. When the concentration of the mediator is large $\varphi/(\varphi + 1) \sim 1$, so that its maximum amplitude (namely, at $t_{\max}$, when $f = 1$) relative to the microband current is not affected by increasing the mediator concentration. To evaluate the time dependence of this major contribution, one needs to evaluate first the variations of L/g with time, since f is critically dependent on this term [see Eq. (21), and Figure 2c].

To determine the variations of L/g we need first to evaluate $V_{\max}$. From the discussion in section on electrochemical kinetics above, at each time $\mathrm{d}h/\mathrm{d}L = k^h_{\mathrm{av}}/k^L_{\mathrm{av}}$, so that from Equation (12), $V_{\max} = \rho c(k^L_{\mathrm{av}}h + k^h_{\mathrm{av}}L)$. Assuming that ohmic drop and accumulations of defects do not significantly vary with time (vide infra), $k^h_{\mathrm{av}}/k^L_{\mathrm{av}}$ is approximately a constant, so that $h \approx (k^h_{\mathrm{av}}/k^L_{\mathrm{av}})L$, and the carbonized cross-section is an elliptic quadrant ($\rho \approx \pi/4$). Hence Equation (28) may be derived.

On the other hand, the volume of the carbonized PTFE tracks the increase of Q^{PTFE}, the charge due to the catalytic current $I^{\mathrm{PTFE}} = I - I_{\mathrm{band}}$. Noting that $\mathrm{d}h/\mathrm{d}L = k^h_{\mathrm{av}}/k^L_{\mathrm{av}}$ so that $h \approx (k^h_{\mathrm{av}}/k^L_{\mathrm{av}})L$, one obtains (note that cathodic currents are negative, and that the cross-section of the carbonized zone is an elliptic quadrant, *vide supra*) Equation (29). Taking advantage of Equations (5), (26) and (27), one gets

$I^{PTFE} = (I - I_{band}) = -(2+\delta)Fl(\Omega V_{max})(1+\varphi f)$, and obtains Equation (30) finally by combination of Equations (28) and (29).

$$V_{max} \approx (\pi/2)c\,k^h_{av}L = (\pi/2)c\,k^L_{av}h \quad (28)$$

$$(\pi/2)(2+\delta)Fcl(k^h_{av}/k^L_{av})L(dL/dt) = -I^{PTFE} = -(I - I_{band}) \quad (29)$$

$$d(L/g)/[1 - f + \Lambda f(g/L)] = (\Omega k^L_{av}/g)\,dt \quad (30)$$

Note that this differential equation does not assume any constraint on k^L_{av}, since it requires only that k^h_{av}/k^L_{av} is constant, but not a constancy of each rate constant. In Equation (30), $\Lambda = (1+\varphi)(L/g)$ is a dimensionless parameter independent of L, given by Equation (31) [compare with Eq. (27) and (28)]. Since we are investigating the behavior for $t > t_{max}$, $(Dt)^{1/2}$ is sufficiently large for $\Phi^*(p)$ and $\Phi^*(p^{app})$ to have reached their convection-controlled limits. Therefore, the expression of f in Equation (21) simplifies to that given in Equation (32), in which Ω^{app}/Ω may be approximated [see Eq. (10)] by $(\Delta_{conv} + \pi g/2)/(\Delta_{conv} + \pi g/2 + \pi L/2) = 1/[1 + (1-\Omega)L/g]$.

$$\Lambda = (2/\pi)(c_M/c)[n/(2+\delta)]\,\vartheta_{w/g}(D/k^h_{av}g) \quad (31)$$

$$f \approx (\vartheta_{w/g}{}^{app}/\vartheta_{w/g})(\Omega^{app}/\Omega) \quad (32)$$

Equation (30) is a differential equation with separate variables and can be easily integrated numerically for any selected function $\Lambda(t)$. However, it is interesting to note (Figure 2c) that when L/g increases, $(\vartheta_{w/g}{}^{app}/\vartheta_{w/g})$ decays much more slowly than $1/(1+L/g)$. Therefore, provided that $(1-\Omega)$ is not too small, $f \approx 1/[1+(1-\Omega)L/g]$ is a convenient approximation over the range of experimental interest. Using this approximation, and introducing the dimensionless length $\lambda = L/g$, and the dimensionless time $\tau = (\Omega k^L_{av}/g)t$, Equation (30) is rewritten as Equation (33), in which ε^* and Λ^* are defined by Equations (34) and (35).

$$d\lambda\,[\lambda(\varepsilon^* + \lambda)/(\Lambda^* + \lambda^2)] = d\tau \quad (33)$$

$$\varepsilon^* = 1/(1-\Omega) \quad (34)$$

$$\Lambda^* = \Lambda/(1-\Omega) = [2n/\pi(2+\delta)](c_M/c)\,\vartheta_{w/g}(k^L_{av}/k^h_{av})(D/k^L_{av}g)/(1-\Omega) \quad (35)$$

Hence, Equation (36) is obtained, whose analytical integration is straightforward whenever Λ^* is time independent, that is, whenever k^L_{av} is constant (vide infra). This integration affords the sought relationship between $L = g\lambda$, $h = (k^h_{av}/k^L_{av})g\lambda$, and the time $t = \tau(g/\Omega k^L_{av})$ [Eq. (37)]. Based upon the solution in Equation (37) (or its numerical equivalents whenever the variations of $\vartheta_{w/g^{app}}/\vartheta_{w/g}$ cannot be neglected, or whenever k^L_{av} varies with time, vide infra), the analytical variations of L/g can be predicted, as shown in Figure 4a.

$$d\lambda + \varepsilon^*[\lambda d\lambda/(\Lambda^* + \lambda^2)] - \Lambda^*[d\lambda/(\Lambda^* + \lambda^2)] = d\tau \quad (36)$$

$$\tau = \lambda + (\varepsilon^*/2)\ln(1 + \lambda^2/\Lambda^*) - \Lambda^{*1/2}\tan^{-1}(\lambda/\Lambda^{*1/2}) \quad (37)$$

At short times, a first order development of Equation (37) affords $\lambda = (2\tau\Lambda^*/\varepsilon^*)^{1/2} = (2\Lambda\tau)^{1/2}$, which gives Equation (38).

$$L = (k^L_{av}/k^h_{av})h = \{[4n/\pi(2+\delta)]\,\vartheta_{w/g}\Omega\,(k^L_{av}/k^h_{av})\}^{1/2}(c_M/c)^{1/2}(Dt)^{1/2} \quad (38)$$

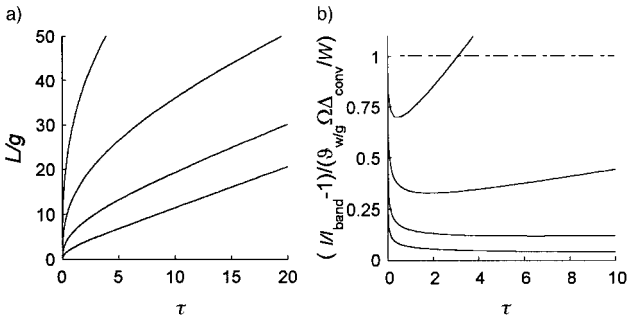

Figure 4. Predicted variations of a) the lateral length L of the carbonized zone according to Equation (37), and of b) the current function $(I/I_{band} - 1)$ according to Equation (40), as a function of the dimensionless time $\tau = (\Omega k^L_{av}/g)t$, for different values of Λ^* (ε^* is kept constant at 2, which corresponds to $\Omega = 0.5$). From top to bottom: $\log(\Lambda^*) = 4$, 3, 2, and 1. The horizontal dashed line in b) indicates the limit above which Equation (40) is no longer valid, so that $(I/I_{band} - 1)$ remains poised at $\vartheta_{w/g}(\Omega\Delta_{conv}/w)$ (see text).

This shows that at short times both L and h increase as $t^{1/2}$; this is also observed under the low-current regime, albeit for completely different reasons. Also, it is interesting to note that the rate of lateral increase does not depend on k^L_{av}, the heterogeneous rate of reduction of CF_2 bonds, but on (k^L_{av}/k^h_{av}). This occurs because at these short times, the fast lateral growth is essentially controlled by the solution–diffusion by-pass and the corresponding charge Q^{PTFE} is modulated between increses in L and h as imposed by the ratio k^L_{av}/k^h_{av}. It is also interesting to note that in this short time limit, V_{max} varies also as $t^{1/2}$, since this parameter is proportional to $k^h_{av}L + k^L_{av}h$ [Eq. (28)].

At long times, Equation (37) simplifies into $\lambda \to \tau$, and hence Equation (39) is obtained.

$$L = (k^L_{av}/k^h_{av})h \to \Omega k^L_{av}t \quad (39)$$

Equation (39) reveals that in the long-time limit, both L and h grow linearly with the time and that their individual rates are proportional to their respective heterogeneous rate constants. This reflects the suppression of the solution–diffusion by-pass because L has become much larger than the slowly expanding (namely, $\propto \ln t$[7, 12, 13]) solution–diffusion layer surrounding the microband generator. The expansion of the carbonized zone occurs then exclusively through the electronic conduction inside it, the solution diffusion serving now solely to *feed* the corresponding charge into the carbonized zone by shuttling the reduced mediator species over the gap g.

It is also interesting to note that under these conditions, V_{max} tends to vary linearly with the time, since this parameter is proportional to $k^h_{av}L + k^L_{av}h$ [Eq. (28)]; thus, $V_{max} \to \Omega(\pi/2)c\,(k^h_{av}k^L_{av}t)$. Therefore, $[(I/I_{band})^{\infty} - 1]$ which is proportional to V_{max} [Eq. (22)] tends also to vary linearly with the time. Evidently, this situation cannot be maintained for ever because the current function $(I/I_{band} - 1)$ cannot exceed its maximum value, namely, $\vartheta_{w/g}(\Omega\Delta_{conv}/w)$, achieved for a perfect generator–collector assembly under convection-controlled conditions [note that this is equivalent to the condition $\varphi \geq 0$ in Eq. (27), vide supra]. This limit imposes [vide infra,

0947-6539/00/0605-0828 $ 17.50+.50/0 Chem. Eur. J. 2000, 6, No. 5

Eq. (40)] that $1+\lambda^2/\Lambda^* \le 1+\lambda/\varepsilon^*$. The corresponding binomial equation has two roots. One, $\lambda=0$, features the short-time boundary [namely, t_{max} in the present context, see Eq. (26)]. The other, $\lambda=\Lambda^*/\varepsilon^*$, corresponds to the sought limit. Above this value, the current function $(I/I_{band}-1)$ remains poised at $\vartheta_{w/g}(\Omega\Delta_{conv}/w)$ and the system has returned to a low-flux regime, so L and h shift toward a variation with the square root of time.

Noting that owing to Equation (33), when $L(t)$ is known, the current follows readily from Equations (29) and (5). This is rewritten in terms of τ and λ as follows in Equation (40), in which $\lambda(\tau)$ is given by Equation (37). At short times, $\lambda \rightarrow (2\tau\Lambda^*/\varepsilon^*)^{1/2}$ to give Equation (41), in which the coefficient β is given by Equation (42).

$$I/I_{band}-1=[\vartheta_{w/g}(\Omega\Delta_{conv}/w)\lambda(d\lambda/d\tau)]/[\Lambda^*(1-\Omega)] = \vartheta_{w/g}(\Omega\Delta_{conv}/w)[(1+\lambda^2/\Lambda^*)/(1+\lambda/\varepsilon^*)] \quad (40)$$

$$I/I_{band}-1 \rightarrow \vartheta_{w/g}(\Omega\Delta_{conv}/w)/(1+\beta t^{1/2}) \quad (41)$$

$$\beta=(1-\Omega)\{\vartheta_{w/g}\Omega(k_{av}^L/k_{av}^h)(c_M/c)(D/g^2)[4n/\pi(2+\delta)]\}^{1/2} \quad (42)$$

In Equation (42) k_{av}^L/k_{av}^h is a constant. The limit at $t=0$ (namely, $t=t_{max}$) of Equation (41) is $(I/I_{band}-1)=\vartheta_{w/g}(\Omega\Delta_{conv}/w)$, in agreement with Equation (26), since $f=1$ at $t=t_{max}$ by definition. Interestingly, since $\beta \propto c_M{}^{1/2}$, $I/I_{band}-1$ decays the faster the greater the concentration of mediator. In other words, the larger the mediator concentration, the smaller the duration of the solution–diffusion by-pass. Importantly, this shows that at large mediator concentration the role of the solution–diffusion process may be suppressed by, or at least strongly convoluted with, the rising part of the current, which features the establishment of the diffusional cross-talk over the insulating gap g [Eq. (25)].

At long times, $\lambda \rightarrow \tau$, so that, Equations (43) and (44) can be derived from Equation (39). These equations predict that $I/I_{band}-1$ varies linearly with the time.

$$I/I_{band}-1 \rightarrow \vartheta_{w/g}(\Omega\Delta_{conv}/w)(\Omega k_{av}^L/\Lambda g)t \quad (43)$$

$$I/I_{band}-1 \rightarrow \{[\pi(2+\delta)/2n](\Delta_{conv}/w)\Omega^2\}(k_{av}^L k_{av}^h/D)(c/c_M)t \quad (44)$$

This is a consequence of the limit of Equation (26) when one introduces V_{max} given in Equation (28). However, as explained above, such a linear behavior cannot be sustained for ever, even if k_{av}^L and k_{av}^h maintain their values indefinitely. In other words, while the times elapses V_{max} increases, so that the system shifts progressively towards a situation analogous to that described in the low-flux regime. Then, $(I/I_{band}-1) \rightarrow \vartheta_{w/g}(\Omega\Delta_{conv}/w)$, and L and h tend to vary with the square root of time. The transition time t_{trans} at which this change of regime occurs is given by Equation (45) in which the limit in Equation (44) is equated to $\vartheta_{w/g}(\Omega\Delta_{conv}/w)$.

$$t_{trans}=(D/k_{av}^L k_{av}^h)(c_M/c)\vartheta_{w/g}/[\Omega\pi(2+\delta)/2n] \quad (45)$$

Thus Equation (44) is valid [as is Eq. (39)] for $t \le t_{trans}$, while $(I/I_{band}-1)=\vartheta_{w/g}(\Omega\Delta_{conv}/w)$ is valid for $t \ge t_{trans}$.

Figure 4b represents the variations of $(I/I_{band}-1)$ based on Equation (40), assuming that the establishment of the diffusional cross-talk over the gap insulator is achieved much faster than the initial decay of the current. The horizontal limit corresponds to the diffusion-limited behavior, namely, $(I/I_{band}-1)=\vartheta_{w/g}(\Omega\Delta_{conv}/w)$, which is reached for $t \ge t_{trans}$. However, as noted above, this limit supposes that k_{av}^L and k_{av}^h maintain their values indefinitely, that is, that ohmic drop plays no significant role (vide infra).

Results and Discussion

The following mediators have been investigated: phtalonitrile ($E^0=-1.50$ V vs. SCE), 4-cyanopyridine ($E^0=-1.70$ V vs. SCE), pyridazine ($E^0=-2.10$ V vs. SCE), 4-phenylpyridine ($E^0=-2.14$ V vs. SCE), benzonitrile ($E^0=-2.27$ V vs. SCE), and naphthalene ($E^0=-2.47$ V vs. SCE). Tests were performed with mediator concentration of approximately 20 mM in DMF/0.1M NBu_4BF_4. Except for the benzonitrile and naphthalene mediators we observed no amplification of the band current nor any visible carbonization of the PTFE adjacent to the gap region. For benzonitrile and naphthalene both effects were observed, indicating that a potential in excess of -2.15 V versus SCE is required to drive efficiently the carbonization process. This is clear evidence that the reductive driving force plays a crucial role in the carbonization process, and that a potential drop from -2.27 V versus SCE (benzonitrile) to -2.15 V versus SCE (4-phenylpyridine) is sufficient to impede the process. In this respect, naphthalene appears as a better mediator than benzonitrile. However, since this work is mostly focused to provide a physicochemical rationale of the dynamics and kinetics of the subtle processes involved, we prefer to rely on benzonitrile. Indeed, this allowed better measurements because the residual currents play a minor role, since its lower standard potential allowed lesser electrode potentials to be used.

Diffusion at the band: In this work, we needed to explore the behavior at long duration times as well as rather important concentrations of mediator. We had therefore to establish the diffusional behavior at the microband alone under these unusual conditions where convective transport prevails [see Eq. (5)]. For this we relied on the control devices, in which the PTFE was substituted by an inert glass plate. Figure 5a shows

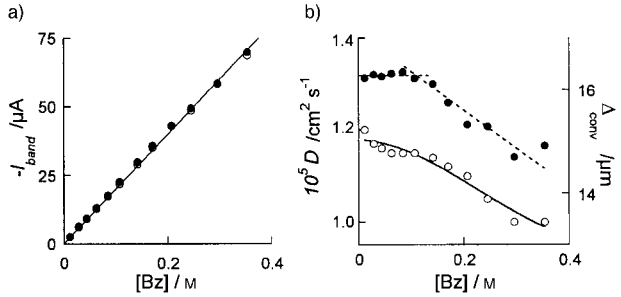

Figure 5. Gold microband ($w=10$ µm, $l=3$ mm) operating alone (control device) in benzonitrile solutions in DMF, 0.2 M NEt_4BF_4. a) Variations of the chronoamperometric steady state plateau current ($E=-2.4$ V vs. SCE) at $t=100$ (solid circles) or 600 s (open circles). b) Variations of the benzonitrile diffusion coefficient (open circles) or of the parameter Δ_{conv} (filled circles) as a function of the benzonitrile concentration.

that in the range of interest ($t > 30$ s) the chronoamperometric band current varies almost linearly with the concentration and does not depend on time; this is in agreement with the formulation in Equation (5). By using this equation, an average value of $D(w/\Delta_{conv}) = 7 \times 10^{-6}$ cm^{2}s^{-1} could be determined over the whole range of experimental conditions investigated here. Determination of D as a function of benzonitrile concentration was then performed by relying on chronoamperometry at short timescales ($t < 50$ ms), at which the band current follows a Cottrell behavior.[12, 13] From the linear regressions (data not shown) of the current versus $t^{-1/2}$, the parameter wD could be determined at each concentration.[7, 14] Since $w = 10$ μm is known independently, this enabled the determination of D and hence that of Δ_{conv} for each benzonitrile concentration (Figure 5b). Under usual electrochemical conditions[17], D and Δ_{conv} have to be independent of the substrate concentration c_{Bz}. Yet, this is no longer true when the mediator is sufficiently concentrated to affect the viscosity and local hydrodynamics[20–22], as is considered here. Then these parameters are expected to vary with c_{Bz}, as observed in Figure 5b and in agreement with previous reports.[19–22, 25]

Effect of the mediator concentration: Figure 6a represents typical experimental variations of $(I/I_{band} - 1)$ with the time as a function of c_{Bz}. In Figure 6a, the supporting electrolyte is NEt_4BF_4 (0.2 M), but qualitatively identical results are obtained when the supporting electrolyte cation or its concentration is changed (vide infra). In agreement with the theory developed above, one observes two different limiting behaviors when c_{Bz} is increased.

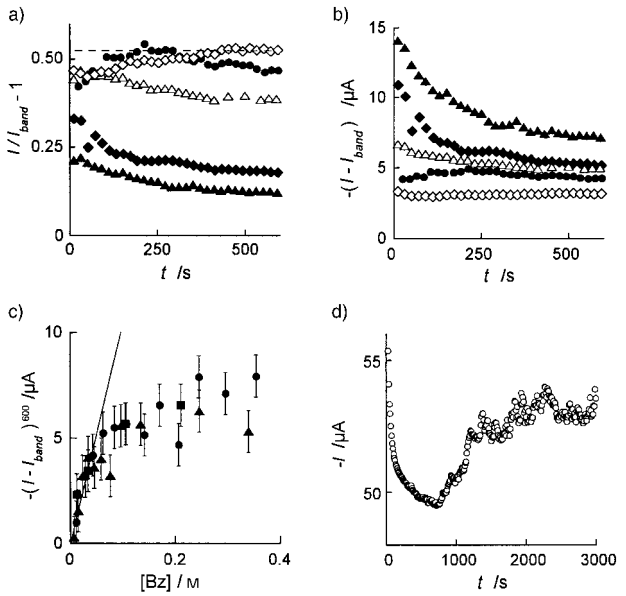

Figure 6. Gold microband ($w = 10$ μm, $l = 3$ mm) operating near a PTFE block ($g = 10$ μm) for different benzonitrile concentrations in DMF, 0.2 M NEt_4BF_4. The microband potential was set at $E = -2.4$ V vs. SCE. a) and b) Variations of the microband current, I, as a function of time for different mediator concentrations: 0.030 (open diamonds), 0.045 (solid circles), 0.065 (open triangles), 0.14 (solid diamonds) and 0.30 M (solid triangles). I_{band}: current observed under the same conditions when the microband performs alone (control device, Figure 5). c) Variations of the current measured at $t = 600$ s as a function of the benzonitrile concentration. d) Variations of the microband current, I, as a function of time over a large timescale for large mediator concentrations (data shown: [Bz] = 0.21 M). The horizontal dashed line shown in a) at $(I/I_{band} - 1) = 0.52$, or the solid line in c) feature the limit for a perfect collector–generator assembly of identical dimensions (see text).

When c_{Bz} is small (approximately, $c_{Bz} < 75$ mM), the current rises quickly to reach a plateau at $(I/I_{band} - 1) \approx 0.52$ (Figure 6a). This value is extremely close to that (0.63) predicted from the convection-controlled limit of Equation (16) for $w = g = 10$ μm (namely, $\vartheta_{w/g} = 0.78$[7]) and $\Delta_{conv} \approx 16$ μm as determined above (Figure 5b). This shows that $\Omega^{exp} = 0.42$ instead of $\Omega = 0.50$ as predicted by Equation (10). Such a difference of approximately 15% is extremely satisfactory considering the series of approximations leading to Equation (10). In the following we therefore use the experimental Ω value ($\Omega^{exp} = 0.42$).

At higher concentrations of mediator (approximately, $c_{Bz} > 100$ mM), and in qualitative agreement with the theoretical expectations (compare Figure 4b), one observes that over the limited timescale shown in Figure 6a, $(I/I_{band} - 1)$ rises initially, but immediately decays so as to reach an horizontal limit (vide infra), which is lower than that observed at low concentrations. Furthermore, the larger c_{Bz}, the smaller this limit is.

This dichotomy is better seen by plotting the current variations in the form of $I^{PTFE} = (I - I_{band})$, as in Figure 6b, or by considering the value of I^{PTFE} at a sufficiently long time as a function of c_{Bz}, as shown in Figure 6c for $t = 600$ s. This latter plot shows that at low values of c_{Bz}, $I^{PTFE} = (I_{band} - I)$ varies linearly with c_{Bz}, with the expected slope [Eq. (16)]. Conversely, at larger concentrations, the limit of $I^{PTFE} = (I_{band} - I)$ becomes almost independent of c_{Bz}. Noticeably, in this high concentration range, I^{PTFE} values are more dispersed from run to run than at low concentrations (vide infra). Finally, for large benzonitrile concentrations, examination of the current variations over a much wider time domain (Figure 6d) shows that, in qualitative agreement with the theoretical expectations (Figure 4b), the current grows again to eventually reach a plateau limit.

This dichotomy as a function of c_{Bz}, is also observed when one considers the time variations of the length (L) and thickness (h) of the carbonized zone for small and large benzonitrile concentrations. L could be determined by measuring the lateral progression of the carbonized zone in situ with a microscope, while the electrochemical reaction proceeds (Figure 1a). Figure 7 represents a set of microscopic views of the carbonized zone taken at different operation times for low and high concentrations. Based on the optically measured L values and the charge $Q^{PTFE}(t)$ consumed, the variations of $h(2 + \delta)c$ could be reconstructed by assuming only a given shape for the cross-section of the carbonized zone. In the following, based on the above theoretical results, we assumed that this is an elliptic quadrant of surface area $(\pi/4)Lh$, and so Equation (46) was obtained.

$$h(2+\delta)c = -Q^{PTFE}(t)/\left(\frac{\pi F l L}{4}\right) = \frac{4}{\pi F l L}\int_0^t (I_{band} - I)\mathrm{d}t \qquad (46)$$

Figures 8a and 8b show typical variations of L and $h(2 + \delta)c$ under the low- and high-concentration regimes, respectively.[26] As predicted by the above analysis, at low mediator

0947-6539/00/0605-0830 $ 17.50+.50/0 Chem. Eur. J. 2000, 6, No. 5

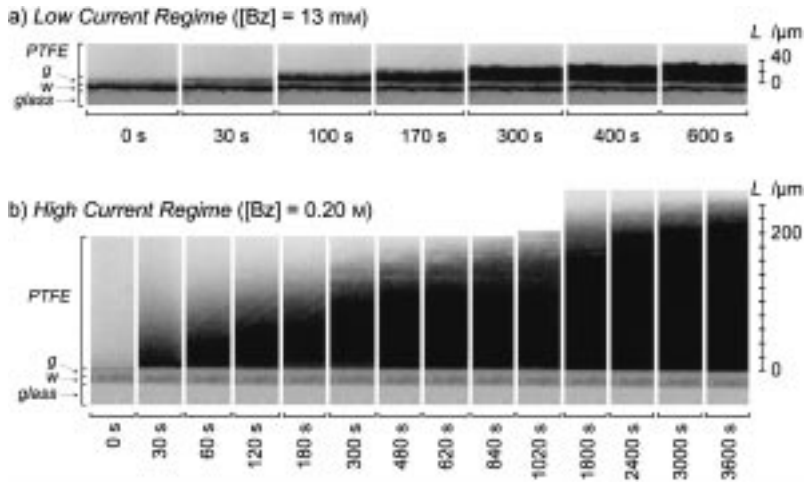

Figure 7. Microscopic views recorded in situ, showing the time progression of the carbonized zone under the two different current regimes. The views where taken at the time indicated with the same magnification and their contrast (as well as the lighting angle) adjusted to represent the most accurately the intensity of carbonization (note that these adjustments are not adequate to represent the microband and insulating gap precisely). The corresponding $L(t)$ variations are shown in Figures 8a and 8b, respectively.

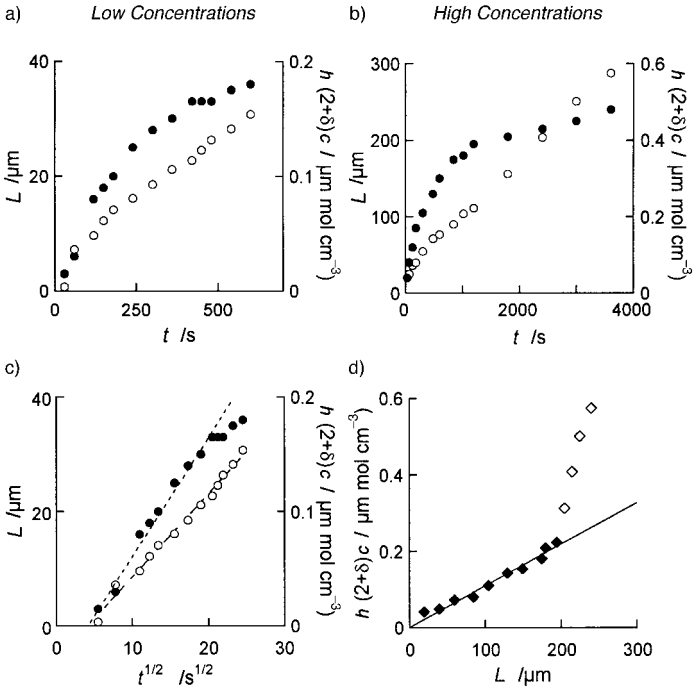

Figure 8. Gold microband ($w = 10$ µm, $l = 3$ mm) operating near a PTFE block ($g = 10$ µm) for two different benzonitrile concentrations in DMF, 0.2 M NEt_4BF_4. The microband potential was set at $E = -2.4$ V vs. SCE. Variations of the lateral (L, solid circles) and in-depth (h, open circles) progression of the carbonized zone for low ([Bz] = 0.013 M for a and c) and high ([Bz] = 0.19 M for b and d) concentration of the benzonitrile mediator, as determined from microscopic views (L, Figure 7) or computed (h) by using Equation (46). a) and b) Variations of L and $h(2+\delta)c$ (see text) with the operation time. c) Plot of the data shown in a) as a function of the square root of the time. d) Plot of the data shown in b) to stress the constancy of σ_0 (see text) for the data represented by solid symbols ($\sigma_0 =$ 1.1 M for $L \leq 200$ µm).

concentration, both L and h vary linearly with the square root of time (Figure 8c), so that $L = (\kappa_L t)^{1/2}$ and $h = (\kappa_h t)^{1/2}$, with $\kappa_L = 4.2 \times 10^{-8}\,\mathrm{cm^2 s^{-1}}$ and $c^2(2+\delta)^2\kappa_h = 5.3 \times 10^{-13}\,\mathrm{mol^2 cm^{-4} s^{-1}}$. Since δ is almost unity and c is almost equal to the concentration of CF_2 groups in PTFE (namely, 44 M), κ_L is approximately 600 to 1400 times larger than κ_h. Such a figure is in agreement with the expected, more difficult, vertical diffusion–migration in the bulk material (vide supra). In addition, Figure 8c shows that the PTFE carbonization occurs with a approximately 30 s delay, a number which is in full agreement with the duration of the rising portion of the current in Figure 6a and of the convective regime (i.e., $\underline{p} \leq \underline{p}_{\mathrm{conv}}$, 33 s). This delay is required for the full establishment of the convection-controlled diffusional cross-talk over the insulating gap, so that the function $\Phi(\mathrm{p})$ reaches its maximum limit (Figure 2a).

At larger mediator concentration, L and h vary much more rapidly, and $L(t)$ variations qualitatively resemble those predicted in Figure 4a. Furthermore, as predicted for a constant value of $k^h_{\mathrm{av}}/k^L_{\mathrm{av}}$, the vertical propagation tracks the lateral one (Figure 8d). $h(2+\delta)c/L$ is approximately a constant over a significant time duration [solid symbols: $(2+\delta)$-$c(k^h_{\mathrm{av}}/k^L_{\mathrm{av}}) = 1.1 \times 10^{-3}\,\mathrm{mol\,cm^{-3}}$ in Figure 8d]. Yet, in all experiments, we observed that after a few thousand seconds, $h(2+\delta)c/L$ increases sharply and deviates from linearity (vide infra). This is apparent in Figure 8d for $L > 200$ µm (open symbols). Although this phenomenon proved general and occurred always when L reaches a few hundred micrometers, the exact L value at which this disruption arose was irreproducible from run to run. We are therefore inclined to ascribe the occurrence of this phenomena to statistical defects in the PTFE; these mostly affect the lateral rate constant k^L_{av}.[26]

Quantitative treatment of the data obtained in the high-current regime: For high fluxes of mediator radical anion, the validity of the analytical theory developed in the section on large reducing fluxes requires that i) the ratio $k^h_{\mathrm{av}}/k^L_{\mathrm{av}}$ of the average heterogeneous rate constants is constant and that ii) k^L_{av} is invariant with time. Plots such as that shown in Figure 8d establish that while $(2+\delta)c(k^h_{\mathrm{av}}/k^L_{\mathrm{av}})$ may vary from one experiment to another,[26] for each given experiment the first hypothesis has some experimental validity provided that the extension of the carbonized zone is not too large (namely, L is less than a few hundred micrometers). This prompted us to examine if the second hypothesis is also sound, that is, if a quantitative agreement could be found between the present model and the experimental data.

The dimensionless formulation of Equation (37) is interesting from a theoretical point of view, because it represents easily the conjugated effect of several independent experimental parameters [compare, for example, the expression of Λ in Eq. (31)]. However, from an experimental point of view this dimensionless formulation presents some difficulties. So,

Equation (37) is experimentally more useful when it is rewritten in its dimensioned [Eq. (47)], in which $\omega_1 = 1/\Omega$, $\omega_2 = g/[2(1-\Omega)]$, and $\sigma = g\Lambda^{*1/2}$.

$$t = \omega_1[L + \omega_2 \ln(1 + L^2/\sigma^2) - \sigma \tan^{-1}(L/\sigma)]/k_{av}^L \quad (47)$$

The parameters $\omega_1 \approx 2.4$, and $\omega_2 \approx 8.5 \times 10^{-4}$ cm are readily obtained experimentally, since the experimental gap $g = 10^{-3}$ cm is known and $\Delta_{conv} \approx 1.6 \times 10^{-3}$ cm or $\Omega^{exp} = 0.42$ are available independently (vide supra). σ depends on both experimentally known parameters and on unknown ones (namely, $(2+\delta)$, c and k_{av}^h): $\sigma = \{(2nDc_M g/\pi c)\,\vartheta_{w/g}/[(1-\Omega)-(2+\delta)k_{av}^h]\}^{1/2}$. In this respect, it is interesting to note that the experimental determination of the vertical propagation through Equation (46) affords the value of $(2+\delta)hc$ directly, so that for any given experiment, $\sigma_0 = (2+\delta)hc/L = (2+\delta)-ck_{av}^h/k_{av}^L$ is directly determined from the slope of plots like that shown in Figure 8d. Thus, σ is best rewritten as $\sigma = \omega_3(c_M/\sigma_0 k_{av}^L)^{1/2}$, in which σ_0 is the slope of the experimental variations of $4Q^{PTFE}/(\pi l^2 FL) = (2+\delta)hc$ *versus* L, and $\omega_3 = [(2nDg/\pi)\,\vartheta_{w/g}/(1-\Omega)]^{1/2}$ is known experimentally, that is, $\omega_3 \approx 9.6 \times 10^{-5}\,cm^{3/2}s^{-1/2}$, for $D \approx 1.1 \times 10^{-5}\,cm^2 s^{-1}$, $w = g = 10^{-3}$ cm (i.e., $\vartheta_{w/g} \approx 0.78$), $\Delta_{conv} \approx 1.6 \times 10^{-3}$ cm, and $\Omega = \Omega^{exp} = 0.42$. Therefore, the fit of the experimental $L(t)$ variations through Equation (47) formally requires the adjustment of a single parameter, namely, k_{av}^L, since all the other parameters are known or determined independently.

Similarly, Equation (40) is best rewritten as Equation (48), in which $\omega_4 = \vartheta_{w/g}(\Omega\Delta_{conv}/w) \approx 0.52$ is known independently from the experimental long-time limit of $(I/I_{band} - 1)$ measured in the low-concentration regime (see e.g., Figure 6a).

$$I = I_{band}[1 + \omega_4(1 + L^2/\sigma^2)/(1 + L/2\omega_2)] \quad (48)$$

I_{band} is also known independently (Figure 5a). Equation (48) shows then that the comparison between the experimental current and the predicted one also requires only the adjustment of the single parameter k_{av}^L.

The results of this procedure are illustrated in Figure 9 for two runs corresponding to nearly identical conditions. It is observed that the model predictions and the experimental observations are qualitatively consistent but that the agreement is far from excellent. This can be easily explained by the fact that even if the model developed here is already rather cumbersome, it relies on an extreme simplification of the phenomena that are involved. The model relies on two crucial hypothesis (see also ref. [26]). The hypothesis regarding the constancy of $c(2+\delta)k_{av}^h/k_{av}^L$ could be verified independently, at least in a large useful domain (compare e.g., Figures 8d, 9a, and 9b). The second one amounts to the consideration that k_{av}^L is constant. However, as discussed above, it is probable that ohmic drop affects this parameter so that k_{av}^L decreases with L.

The hypothesis on the constancy of k_{av}^L was introduced to decrease the number of parameters at hand (vide infra) and to facilitate the time integration of Equation (36), since this resulted in a constant parameter Λ^*. In this respect, it is worth noting that Equation (40) is a differential equation relating $(I/I_{band} - 1)$ to $L(dL/dt)$. So, its validity does not require that Λ^* is constant. In other words, the time variations of Λ^*, and

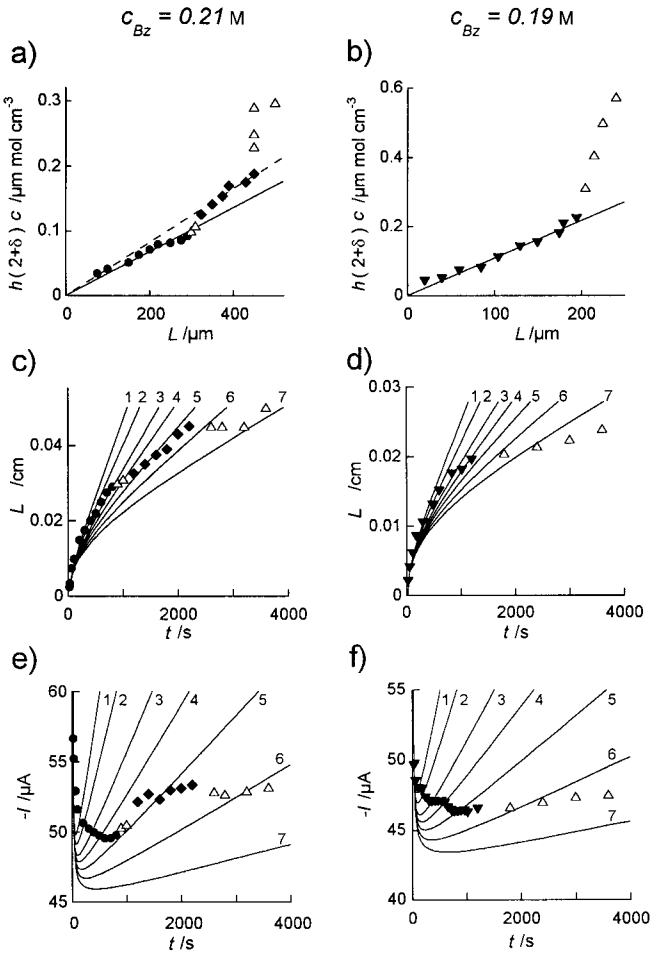

Figure 9. Comparison between the theoretical predictions and two data sets obtained for two runs performed under almost identical conditions. Gold microband ($w = 10$ μm, $l = 3$ mm) operating near a PTFE block ($g = 10$ μm). Benzonitrile mediator in DMF, 0.2 M NEt_4BF_4 ; [Bz] = 0.21 (a,c,e) or 0.19 M (b,d,f). The microband potential was set at $E = -2.4$ V vs. SCE. a) and b) Variations of $h(2+\delta)c$ vs. L; $\sigma_0 = 3.5 \times 10^{-4}$ (a) and 1.1×10^{-3} (b) (see text). c) and d) Variations of L with the time. e) and f) Variations of the current with the time. In c–f, the data represented by solid symbols represents those for which a linear relationship between $h(2+\delta)c$ vs. L could be observed (see text), and the solid lines represent the variations predicted by Equations (47) or (48): (c,e): $\sigma_0 = 0.35$ M ; $10^5 k_{av}^L = 10$ (1), 8 (2), 6 (3), 5 (4), 4 (5), 3 (6), and 2 cm s^{-1} (7) ; (d,f): $\sigma_0 = 1.1$ M ; $10^5 k_{av}^L = 5$ (1), 4 (2), 3 (3), 2.5 (4), 2 (5), 1.5 (6), and 1 cm s^{-1} (7).

therefore those of k_{av}^L, can be determined experimentally by combining the time variations of $(I/I_{band} - 1)$ and those of L. For this purpose, Equation (40) is best reformulated into its dimensioned form in Equation (48), so that the time variations of $k_{av}^L = (\omega_3^2 c_M/\sigma_0)/\sigma^2$ can be determined for each experiment [Eq. (49)].

$$k_{av}^L = (\omega_3^2 c_M/\sigma_0)\,[(I/I_{band} - 1)\,(1 + L/2\omega_2)/\omega_4 - 1]/L^2 \quad (49)$$

The result of this analysis is represented in Figure 10a for the two series of experiments shown in Figure 9. In each experiment, we restricted to the domain in which $c(2+\delta)k_{av}^h/k_{av}^L$ is constant as deduced from the corresponding plots of $c(2+\delta)h$ versus L (filled symbols in Figures 9a and 9b). It is seen that for each given experiment k_{av}^L does not vary excessively, especially when considering its larger variability

0947-6539/00/0605-0832 $ 17.50+.50/0 *Chem. Eur. J.* **2000**, *6*, No. 5

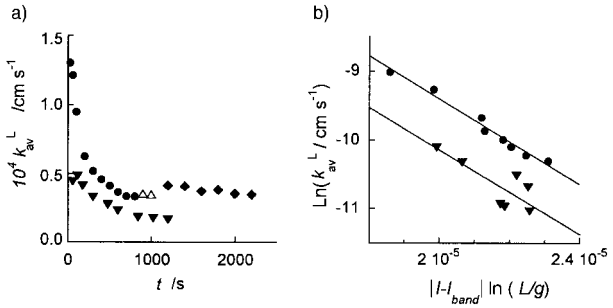

Figure 10. Variations of k_{av}^{L} a) as a function of time or b) as a function of the lateral extension of the carbonized zone for the data shown in the Figure 9 [see text and Eqs. (49) and (51)]. [Bz] = 0.19 (triangles) or 0.21 M (circles). The data represented by solid symbols represents those for which a linear relationship between $h(2+\delta)c$ vs. L could be observed in Figures 9a and 9b, respectively; the data shown by open triangles in Figure 9 were not used, since they did not give rise to such a linear relationship.

from run to run, but it systematically decreases with time. Therefore, the approximation that this parameter is constant during one given experiment is not intrinsically incorrect. We wish to examine hereafter if the decrease of k_{av}^{L} with time may be ascribed to ohmic drop.

Effect of ohmic drop in the high-concentration regime: As k_{av}^{L} is a rate of electron transfer, it must depend exponentially on the locally available driving force.[17] This driving force decreases while the carbonized region extends because of ohmic drop. Therefore we can write Equation (50) in which α

$$k_{av}^{L} = (k_{av}^{L})_0 \exp\{-\alpha[F(E_M - E^0) + |I - I_{band}| R_{av}^{L}]/RT\} \quad (50)$$

is the transfer coefficient, E_M the potential imposed by the mediator couple at the extremity of the carbonized region touching the mylar insulating gap, E^0 the redox potential equivalent to reactions in Equations (14) and (15), $(k_{av}^{L})_0$ the value of k_{av}^{L} at $E_M = E^0$ and at zero current, and R_{av}^{L} the average ohmic resistance of the carbonized zone over the length L. When σ_0 is constant the carbonized zone has a cross-section shaped as an elliptic quadrant with $L \gg h$, so that $R_{av}^{L} \sim (\rho/l)\ln(L/L_0)$, in which ρ is the average resistivity of the carbonized zone and L_0 is close to g (vide supra).[7] This allows to rewrite Equation (50) as Equation (51), in which $\zeta = \ln(k_{av}^{L})_0 - \alpha F(E_M - E^0)/RT$ is a constant.

$$\ln(k_{av}^{L}) \approx \zeta - \rho(\alpha/lRT)[|I - I_{band}| \ln(L/g)] \quad (51)$$

Figure 10b shows that the formulation in Equation (51) agrees satisfactorily with the experimental data, thus supporting that ohmic drop plays a significant role on the propagation of the carbonized zone by controlling the rate of the heterogeneous reductions at the PTFE/carbonized PTFE interface. This important feature may thus explain the increasing deviation between the above model predictions (at constant k_{av}^{L}) and the experimental data when L increases.

As noted above, a variable k_{av}^{L} can be accommodated by the above analysis, but the solution can no more be achieved analytically and requires a numerical solution of Equations (33) and (40). The results of such a procedure are shown in Figure 11 for the set of data shown in Figures 9a, 9c, and 9e. Thus, σ_0 was determined first from the plot in Figure 9a: $\sigma_0 = 0.35$ M (solid circles) or $\sigma_0 = 0.40$ M (solid diamonds); note that the data shown by open triangles in this figure were discarded in this analysis because they did not comply with the condition of a constant σ_0. The variations of k_{av}^{L} with (L/g) were then extracted from the experimental $L(t)$ and I^{PTFE} variations by the above procedure [Eq. (49)]. This yields (Figure 11a) $k_{av}^{L}/(\mathrm{cm\,s^{-1}}) = 8.6\,10^{-4}(L/g)^{-0.97}$ (solid circles) and $k_{av}^{L}/(\mathrm{cm\,s^{-1}}) = 2.6\,10^{-4}(L/g)^{-0.58}$ (solid diamonds). Then Equations (33) and (40) were solved numerically based on all the previously determined parameters (namely, $\omega_1 = 2.4$, $\omega_2 = 8.5 \times 10^{-4}$ cm, $\omega_3 = 9.6 \times 10^{-5}\ \mathrm{cm^{3/2}\,s^{-1/2}}$, and $\omega_4 = 0.52$) for each set of σ_0 and $k_{av}^{L}(L)$ values that correspond to the two series of data shown by solid symbols in Figure 9a. The results of this procedure are presented in Figures 11b and 11c for L and $I^{PTFE} = (I - I_{band})$ variations with time, respectively. As evidenced from this set of figures, the agreement between theory and experiment is extremely satisfactory provided that the ohmic drop limitation is taken into account even through a simplified model. In particular, it is observed that although a small (<15%) change of σ_0 value is observed around $L = 320$ μm in Figure 9a, this transition is not drastically reflected in the time variations of k_{av}^{L} (Figure 11a) or in those of L (Figure 11b). Conversely, this small shift is associated with a sharp transition in the theoretical or experimental variations of $I^{PTFE} = I - I_{band}$ (Figure 11c). This stresses again what we noted already, that is, that the current–time variations are extremely sensitive to small changes in the local surface properties of the PTFE[26] (compare e.g., the different behaviors in Figure 9 for closely identical experimental conditions or the high dispersion of data in Figure 6c) when the system performs in a high-flux regime. However, since this does not severely affect the variations of L, which have become extremely smooth in

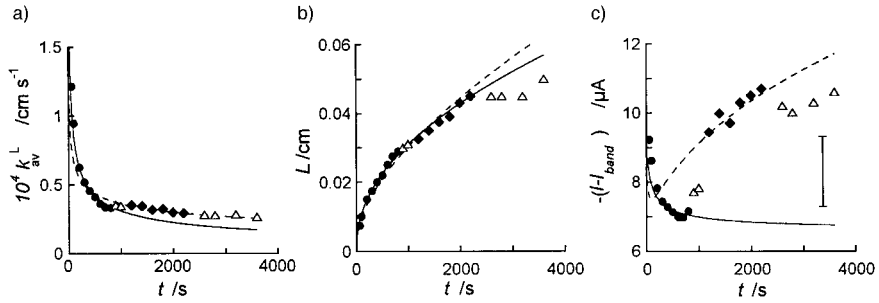

Figure 11. Comparison between experimental variations and simulated ones upon consideration of the effect of ohmic drop. Data are those shown in Figure 9a,c,e and symbols are identical (the data shown by open triangles in Figure 9 were not used in this analysis although they are reported on the present figures, since they did not give rise to a linear relationship for $h(2+\delta)c$ vs. L). Simulations are performed for $\sigma_0 = 0.35$ M and $k_{av}^{L}/(\mathrm{cm\,s^{-1}}) = 8.6 \times 10^{-4}(L/g)^{-0.97}$ (solid circles) or $\sigma_0 = 0.40$ M and $k_{av}^{L}/(\mathrm{cm\,s^{-1}}) = 2.6 \times 10^{-4}(L/g)^{-0.58}$ (solid diamonds) to account for the two values of σ_0 in Figure 9a. Variations of a) $k_{av}^{L}(t)$, b) $L(t)$, and c) $I^{PTFE}(t)$. In c), the vertical segment represents the precision on $(I - I_{band})$ measurement.

this time domain, the experimental implications of these variations are small in terms of surface modifications.

Effect of cation size and concentration of the supporting electrolyte: The above investigation was performed by using a single concentration of supporting electrolyte and a single tetraalkylammonium cation. In this section, we wish to examine qualitatively if changes in the nature of the supporting electrolyte or of its concentration affect the results presented.

Figure 12a shows that the supporting electrolyte concentration does not significantly affect the phenomenon, either in the low or high concentration range. This is true even when the supporting electrolyte concentration is smaller than that

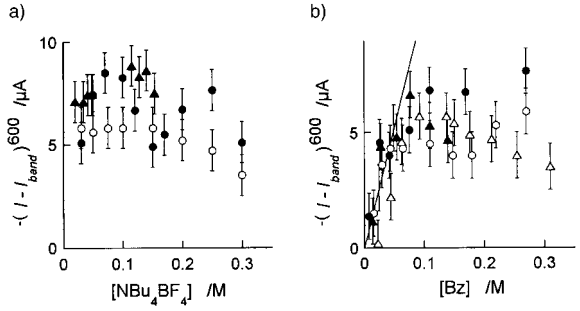

Figure 12. Gold microband ($w = 10$ μm, $l = 3$ mm) operated near a PTFE block ($g = 10$ μm). Benzonitrile mediator in DMF, 0.2 M NEt_4BF_4. The microband potential was set at $E = -2.4$ V vs. SCE. Effect of a) the supporting electrolyte concentration or b) its cation size and concentration on the microband current, I. a) Effect of the NBu_4BF_4 supporting electrolyte concentration for different benzonitrile concentrations: [Bz] = 0.060 (open circles) or 0.10 M (solid circles and solid triangles). b) Comparison of the effect of NBu_4BF_4 (solid symbols) and $NHex_4BF_4$ (open symbols) supporting electrolytes on the variations of the microband current with the benzonitrile concentration ; $[NBu_4BF_4] = 0.10$ (solid circles) and 0.20 M (solid triangles); $[NHex_4BF_4] = 0.10$ (open circles) or 0.20 M (open triangles); compare with Figure 6c for the NEt_4BF_4 supporting electrolyte.

of the mediator. This is easily rationalized by taking into account that since the solution has to remain electroneutral, the supporting electrolyte cation concentration in the diffusion layer is always at least equal to the concentration of the mediator radical anion generated at the microband by ionic enrichment of this region.[19–22, 25] So even when the supporting electrolyte is formally deficient inside the bulk solution, its concentration in the solution range of interest is at least equivalent to that of the mediator radical anion. This phenomenon is now well documented in the literature.[19–22, 25] The same reasoning is also valid inside the PTFE carbonized zone. This explains why the supporting electrolyte concentration does not notably affect the system dynamics. In fact, Figure 12a shows that the variability of the system from run to run affects the data much more significantly.[26]

The size of the cation of the supporting electrolyte was anticipated to have a more pronounced effect, since it is expected to play a crucial role in controlling the mobility of ions inside the carbonized zone [Eqs. (14) and (15)]. Figure 12b shows that as expected, the cation size has almost no effect on the current in the low-concentration regime, since this regime is governed by diffusion into the solution side. Conversely, and as expected, it is found to have a significant effect in the high-concentration regime. Overall, one observes that the larger the cation radius, the smaller the current, and the smaller the concentration at which the system shifts from the low- to the high-concentration regime. However, the effect is not drastic and may even be canceled due to the variability of PTFE[26] (note that each data point in Figure 12b corresponds to a different single experiment). At first glance, this may be a surprizing result, since the size of the supporting electrolyte cation is intuitively expected to alter significantly the rate of transport inside the carbonized layer. However, it is worth recalling that under our experimental conditions, the system behaves under either one of the two following regimes. Under the low-reducing flux regime, the transport inside the carbonized zone plays no kinetic role and just accommodates the flux controlled by the solution diffusional feedback, where the cation size plays no significant role.[19–22, 25] Similarly, the transport inside the carbonized zone cannot play an important kinetic role under the high-flux regime, since then the dynamics of the system are then ruled by the kinetics of the reduction of carbon–fluoride bonds at the moving interface between the fresh and carbonized PTFE, that is, they depend mostly on the intrinsic heterogeneous rate constants of reduction which ought to be immune to the size of the supporting electrolyte cation.[27] In fact, under this high-flux regime, the cation size should have only an indirect incidence on the kinetics by modulating the resistivity [namely, the value of ρ in Eq. (51)] of the n-doped material[1, 4], and, therefore, by modulating the ohmic drop contribution. However, we have shown above that if this effect is certainly observable experimentally, it remains small and is within the range of variability of the experiments.[26]

Conclusion

By using a gold microband electrode we have confirmed that PTFE surfaces can be modified over significant lengths by indirect reduction with the use of a redox mediator. In agreement with previous reports,[1–6] such surface modification affords a carbonized material that presents a significant electronic conduction, so that the carbonization process may propagate well beyond the range available by cylindrical diffusion of the mediator radical anion. Thus the system of the gold microband flanked by the PTFE block and separated from it by an insulating gap behaves as a generator–collector double-band device, in which the constantly enlarging carbonized zone plays the role of the collector electrode. This results in an amplification of the gold microband current because of the constant regeneration of the mediator at the gap outer edge.

Provided that the flux of reducer generated by the gold microband does not exceed the rate at which PTFE can be reduced at the growing interface between the carbonized region and the unaltered PTFE, this type of generator–collector dynamics is sustained for long time periods and allows a continuous extension of the carbonized zone under an apparent diffusion-controlled rate law.

0947-6539/00/0605-0834 $ 17.50+.50/0 *Chem. Eur. J.* **2000**, *6*, No. 5

When the flux of reducer is too large (approximately $c_M \geq 0.1$M for benzonitrile and an electrode potential located on its reduction plateau), the system initially maintains its previous amplification despite the fact that the rate of PTFE reduction is formally too small to accept such a large flux. This occurs because the fraction of mediator radical anion that cannot be oxidized at the gap edge diffuses through the solution and reacts directly with fresh PTFE at the solution/PTFE interface. Thus the carbonization zone now extends through a double mechanism, the diffusion solution pathway by-passing the kinetic saturation at the interface between fresh and carbonized PTFE. However, this situation cannot be maintained during long operation times because the carbonized region elongates faster than the slowly expanding solution cylindrical diffusion layer. Ultimately, no significant flux of radical anion can reach fresh PTFE zones. Then the carbonization process proceeds only through the electronic conduction into the carbonized PTFE and is limited by the rate of heterogeneous reduction. However, since this rate is proportional to the increasing surface area of the interface between fresh and carbonized PTFE, after some time, the current increases again and should return to its initial value. This peculiar behavior is observable experimentally, but only as a trend since in all experiments the carbonization was observed to slow down before this limit is reached. This occurred because of the increasing ohmic drop inside the ever increasing zone of carbonized material; this progressively reduces the available electrochemical driving force for reduction of new carbon–fluorine bonds at the interface between fresh and carbonized PTFE zones.

The conceptually simple model developed here leads to an adequate qualitative description and to a reasonable prediction of all the main dynamic features of the system. Incorporation of the effect of ohmic drop on the variation of the heterogeneous rate constant allowed the quantitative reproduction of the experimental behavior through the empirical adjustment of a parameter $\alpha\rho$, which cumulates the effect of the transfer coefficient α of carbon–fluorine bond reduction and the internal resistivity (ρ) of the carbonized zone.

Acknowledgements

This work was supported in part by CNRS (UMR 8640 "PASTEUR", and ERS 657), by the French Ministry of Research and Education (MENRT), as well as by ENS and ESPCI.

[1] L. Kavan, *Electrochemical Carbonization of Fluoropolymers* in *Chemistry and Physics of Carbon*, *a Series of Advances*, *Vol. 23* (Ed.: P. A. Thrower), Dekker, New York, **1991**, p. 69.
[2] K. Brace, C. Combellas, M. Delamar, A. Fritsch, F. Kanoufi, M. E. R. Shanakan, A. Thiébault, *Chem. Commun.* **1996**, 403.
[3] K. Brace, C. Combellas, M. Delamar, E. Dujardin, F. Kanoufi, M. E. R. Shanakan, A. Thiébault, *Polymer* **1997**, *38*, 3295.
[4] R. H. Dahm, D. J. Baker, D. M. Brewis, L. R. J. Hoy, in *Adhesion*, *Vol. 4* (Ed.: K. W. Allen), Applied Science, London, **1980**, p. 215.
[5] M. Fouletier, PhD Thesis, Grenoble, **1983**.
[6] M. Fouletier, M. Armand, Fr. Pat. 2552092, **1983** [*Chem. Abs.* **1985**, *103*, P178 814b].
[7] B. Fosset, C. Amatore, J. E. Bartelt, A. C. Michael, R. M. Wightman, *Anal. Chem.* **1991**, *63*, 306.
[8] J. E. Bartelt, M. R. Deakin, C. Amatore, R. M. Wightman, *Anal. Chem.* **1988**, *60*, 2167.
[9] T. Varco Shea, A. J. Bard, *Anal. Chem.* **1987**, *59*, 2101.
[10] C. Amatore, A. R. Brown, L. Thouin, J. S. Warkocz, *C. R. Acad. Sci. Paris Ser. IIc* **1998**, *1*, 509.
[11] C. Amatore, L. Thouin, J. S. Warkocz, *Chem. Eur. J.* **1999**, *5*, 456.
[12] M. R. Deakin, R. M. Wightman, C. A. Amatore, *J. Electroanal. Chem.* **1986**, *215*, 49.
[13] "Electrochemistry at Ultramicroelectrodes in Physical", C. Amatore, *Electrochemistry: Principles*, *Methods and Applications* (Ed.: I. Rubinstein), Dekker, New York, **1995**, chapter 4, pp. 131–208.
[14] C. Amatore, M. Azzabi, P. Calas, A. Jutand, C. Lefrou, Y. Rollin., *J. Electroanal. Chem.* **1990**, *288*, 45.
[15] X. Gao, J. Lee, H. S. White, *Anal. Chem.* **1995**, *67*, 1541.
[16] C. P. Andrieux, J. M. Savéant, *Electrochemical Reactions* in *Investigation of Rates and Mechanisms of Reactions*, *Vol. 6* (Ed.: C. F. Bernasconi), Wiley, **1986**, pp. 378–382.
[17] A. J. Bard, L. R. Faulkner, in *Electrochemical Methods*, Wiley, New York, **1980**.
[18] C. Amatore, J. S. Warkocz, unpublished results, **1999**, part of J. S. Warkocz's PhD. thesis.
[19] M. F. Bento, L. Thouin, C. Amatore, *J. Electroanal. Chem.* **1998**, *446*, 91.
[20] M. F. Bento, L. Thouin, C. Amatore, I. Montenegro, *J. Electroanal. Chem.* **1998**, *443*, 137.
[21] C. P. Smith, H. White, *Anal. Chem.* **1993**, *65*, 3343.
[22] C. Amatore, L. Thouin, M. F. Bento, *J. Electroanal. Chem.* **1999**, *463*, 45.
[23] C. Amatore, B. Fosset, K. M. Maness, R. M. Wightman, *Anal. Chem.* **1993**, *65*, 2311.
[24] T. A. Postlethwaite, J. E. Hutchison, R. Murray, B. Fosset, C. Amatore, *Anal. Chem.* **1996**, *68*, 2951.
[25] C. Amatore, B. Fosset, J. E. Bartelt, M. R. Deakin, R. M. Wightman, *J. Electroanal. Chem.* **1988**, *256*, 255.
[26] The experimental determination of L is not so straightforward as implied above. This difficulty is related to the problem in deciding the location of the experimental boundary between the carbonized and unaltered zones on the microscopic views. Figure 7 shows that the boundary is not as abrupt as considered in the model, but consists always of a fringe of gray area. A larger magnification of this intermediate area shows that it consists of black dendritic filaments immersed into the white PTFE, so that the gray shade variations in fact reflect the concentration of the black dendrites. This percolating feature is not significant in the low-concentration regime, but is always distinctly observable in the high-concentration regime. We rationalize this phenomenon by considering that the propagation of the carbonized zone proceeds faster through dendritic pathways in which the electronic conjugation between the reduced chains is the larger and/or the heterogeneous rate of reduction is larger. This percolating feature, which is not accounted for by the present model, may well explain the poor experimental reproducibility from run to run, because each polishing exposes different zones so that each individual experiment may be affected differently by the difficult reproducibility of the polishing conditions. In the experimental determination of $L(t)$ we tried to always select the same density of gray to fix a reproducible carbonized zone "boundary". However, this is not really accurate from run to run, because the gray scale is affected by slight variations in the angle of the light beam with respect to the electrode/PTFE active surface.
[27] a) R. A. Marcus, *J. Chem. Phys.* **1965**, *679*, 43; b) For a recent review and discussion theories of adiabatic heterogeneous electron transfers, see: N. S. Hush, *J. Electroanal. Chem.* **1999**, *460*, 5.

Received: May 19, 1999 [F1793]